nature medicine

The ryanodine receptor store-sensing gate controls Ca^{2+} waves and Ca^{2+}-triggered arrhythmias

Wenqian Chen[1], Ruiwu Wang[1], Biyi Chen[2], Xiaowei Zhong[1], Huihui Kong[1], Yunlong Bai[1,6], Qiang Zhou[1,6], Cuihong Xie[1,6], Jingqun Zhang[3], Ang Guo[2], Xixi Tian[1], Peter P Jones[1,6], Megan L O'Mara[4], Yingjie Liu[1], Tao Mi[1,6], Lin Zhang[1], Jeff Bolstad[1], Lisa Semeniuk[1], Hongqiang Cheng[5,6], Jianlin Zhang[5], Ju Chen[5], D Peter Tieleman[4], Anne M Gillis[1], Henry J Duff[1], Michael Fill[3], Long-Sheng Song[2] & S R Wayne Chen[1,3]

Spontaneous Ca^{2+} release from intracellular stores is important for various physiological and pathological processes. In cardiac muscle cells, spontaneous store overload–induced Ca^{2+} release (SOICR) can result in Ca^{2+} waves, a major cause of ventricular tachyarrhythmias (VTs) and sudden death. The molecular mechanism underlying SOICR has been a mystery for decades. Here we show that a point mutation, E4872A, in the helix bundle crossing region (the proposed gate) of the cardiac ryanodine receptor (RyR2) completely abolishes luminal, but not cytosolic, Ca^{2+} activation of RyR2. The introduction of metal-binding histidines at this site converts RyR2 into a luminal Ni^{2+}-gated channel. Mouse hearts harboring a heterozygous RyR2 mutation at this site (E4872Q) are resistant to SOICR and are completely protected against Ca^{2+}-triggered VTs. These data show that the RyR2 gate directly senses luminal (store) Ca^{2+}, explaining the regulation of RyR2 by luminal Ca^{2+}, the initiation of Ca^{2+} waves and Ca^{2+}-triggered arrhythmias. This newly identified store-sensing gate structure is conserved in all RyR and inositol 1,4,5-trisphosphate receptor isoforms.

Ca^{2+} release from intracellular stores drives many cellular processes[1,2]. This release is generally mediated by two homologous classes of Ca^{2+} channels: RyRs and inositol 1,4,5-trisphosphate receptors (IP3Rs). Cytosolic Ca^{2+} activation of RyRs and IP3Rs is commonly termed Ca^{2+}-induced Ca^{2+} release[1–4]. The possibility of release regulation by store (luminal) Ca^{2+} was first proposed to explain IP3R function[5–8]. Since then, it has become clear that luminal Ca^{2+} also critically controls the cardiac RyR (RyR2)[9–17]. In cardiac muscle cells, Ca^{2+} overload in the sarcoplasmic reticulum (SR) triggers spontaneous RyR2-mediated Ca^{2+} release[3,18–22]. This SOICR can result in Ca^{2+} waves and delayed afterdepolarizations, a major cause of VTs and sudden death[14,23–27]. Analogous mechanisms appear to operate in many other cell types in which spontaneous Ca^{2+} release has an important role in a variety of cellular processes[2,6,7,28,29]. Despite its physiological and pathological importance, the molecular mechanism underlying spontaneous Ca^{2+} release remains largely unknown.

A key feature of SOICR is that it occurs when store Ca^{2+} reaches a critical concentration at which RyR2 channels begin to open[10,13,30,31], but how elevation of store (luminal) Ca^{2+} activates RyR2 is unclear. One proposed mechanism, the 'feed-through' hypothesis, suggests that luminal Ca^{2+} passes through an open RyR2 and acts on the cytosolic Ca^{2+} activation site of the same RyR2 channel through which it just passed[12,32]. However, an accumulating body of evidence indicates that luminal Ca^{2+} activation of a single RyR2 is mediated by a luminal Ca^{2+} sensor that is structurally distinct from the RyR's cytosolic Ca^{2+} activation site [11,17,33–35]. The molecular nature of the luminal Ca^{2+}-sensing mechanism is poorly understood. It is commonly believed that cardiac calsequestrin (CASQ2), a SR luminal Ca^{2+}-binding protein, serves as the key SR luminal Ca^{2+} sensor[17,36]. However, RyR2 in CASQ2-null cardiomyocytes still senses changes in SR luminal Ca^{2+} (ref. 37), indicating that other luminal Ca^{2+}-sensing mechanisms exist. Indeed, purified native or recombinant RyR can sense changes in luminal Ca^{2+} in the absence of CASQ2 (refs. 12,38,39). Thus, RyR2 is also regulated by a luminal Ca^{2+}-sensing mechanism that does not require CASQ2.

In the present study we identified the helix bundle crossing region of RyR2 (its proposed gate) as an essential element of this non–CASQ2 based store (luminal) Ca^{2+}-sensing mechanism. We show that this store Ca^{2+}-sensing gate controls the regulation of RyR2 by luminal Ca^{2+}, the initiation of Ca^{2+} waves and, consequently, Ca^{2+}-triggered VTs.

[1]The Libin Cardiovascular Institute of Alberta, Department of Physiology and Pharmacology, University of Calgary, Calgary, Alberta, Canada. [2]Division of Cardiovascular Medicine, Department of Internal Medicine, University of Iowa Carver College of Medicine, Iowa City, Iowa, USA. [3]Department of Molecular Biophysics and Physiology, Rush University Medical Center, Chicago, Illinois, USA. [4]Department of Biological Sciences and Institute for Biocomplexity and Informatics, University of Calgary, Calgary, Alberta, Canada. [5]Department of Medicine, University of California at San Diego, La Jolla, California, USA. [6]Present addresses: Department of Pharmacology, the State-Province Key Laboratories of Biomedicine-Pharmaceutics of China, Key Laboratory of Cardiovascular Research, Ministry of Education, Harbin Medical University, Harbin, China (Y.B.), Department of Cardiology of Tongji Hospital, Tongji Medical College, Huazhong University of Science and Technology, Wuhan, China (Q.Z. and C.X.), Department of Physiology, University of Otago, Dunedin, New Zealand (P.P.J.), Department of Geriatrics of Tongji Hospital, Tongji Medical College, Huazhong University of Science and Technology, Wuhan, Hubei, China (T.M.), and Department of Pathology and Pathophysiology, Program in Molecular Cell Biology, Zhejiang University School of Medicine, Hangzhou, China (H.C.). Correspondence should be addressed to S.R.W.C. (swchen@ucalgary.ca).

Received 1 September 2013; accepted 3 December 2013; published online 19 January 2014; doi:10.1038/nm.3440

RESULTS

Residue E4872 is essential for RyR2 luminal Ca^{2+} sensing

A number of functional and structural studies[40–44] have suggested that the C-terminal part of the predicted inner helix of the RyR (the helix bundle crossing region) constitutes the ion gate of the channel (**Supplementary Fig. 1**), analogous to the intracellular gates of potassium and sodium channels[45–47]. Notably, a number of negatively charged residues are clustered in or near the proposed ion gate of RyR2 (**Supplementary Fig. 1**). We assessed the functional importance of these negatively charged residues in Ca^{2+} regulation of RyR2 using site-directed mutagenesis and single channel recordings in planar lipid bilayers with K^+ as the charge carrier at −20 mV (cytosolic). The E4872A mutation (but not D4875A, E4878A or E4882A mutation) completely abolished luminal Ca^{2+} activation of single RyR2 channels (**Fig. 1** and **Supplementary Fig. 2**). Single wild-type (WT) RyR2 channels were substantially activated by luminal Ca^{2+} in the presence of ATP and caffeine (**Fig. 1a**,**e**). The WT RyR2 channel can also be activated by luminal Ca^{2+} with[16,39] or without[16,33,39] caffeine being present. As ATP and caffeine each individually enhance RyR2 luminal Ca^{2+} activation[33,39], we used ATP and caffeine together to maximize the Ca^{2+} sensitivity of RyR2 so that even a very small (or residual) luminal Ca^{2+} response of the mutant channels could be detected. In sharp contrast to single WT RyR2 channels, luminal Ca^{2+} (up to 40 mM) did not activate single E4872A mutant channels in the absence or presence of caffeine (**Fig. 1b**,**e**). The E4872A mutant channel was completely unresponsive to luminal Ca^{2+} even in the presence of tenfold higher cytosolic Ca^{2+} (491 nM versus 45 nM) (**Fig. 1c**,**e**). Notably, introduction of a negative charge (G4871E) adjacent to E4872A (resulting in the double mutant G4871E E4872A) largely restored luminal Ca^{2+} activation of E4872A mutant channels (**Fig. 1d**,**e**). Similarly to the E4872A mutation, the isosteric mutation E4872Q abolished or markedly reduced the response of RyR2 to luminal Ca^{2+} activation (**Supplementary Fig. 2**). The removal of fixed negative charges in the internal pore might be expected to alter RyR2 permeation properties. However, the E4872A mutation did not affect single channel conductance in the presence (2.5 mM) or near absence (45 nM) of luminal Ca^{2+} (**Fig. 1f**). These results show that the negative charge at (or near) residue E4872 is essential for luminal Ca^{2+} activation of RyR2.

We assessed the effect of the E4872A and E4872Q mutations on cytosolic Ca^{2+} activation of RyR2 in lipid bilayers (**Fig. 2**). Although totally unresponsive to luminal Ca^{2+}, single E4872A or E4872Q mutant channels remained sensitive to cytosolic Ca^{2+} (**Fig. 2a–c**). However, compared to WT channels, the E4872A and E4872Q channels were less sensitive to activation by cytosolic Ca^{2+} (**Fig. 2d**) and had reduced mean open times (**Fig. 2e**) and increased half-maximum effective concentration (EC_{50}) values (by approximately threefold) of Ca^{2+} activation of [^{3}H]ryanodine binding (from 0.22 μM (WT) to 0.72 μM (E4872A) and 0.58 μM (E4872Q)) (**Fig. 2f**). This result indicates that the E4872A and E4872Q mutations also affect the cytosolic Ca^{2+} activation process. We have previously shown that the E3987 residue is critically involved in cytosolic Ca^{2+} activation of RyR2: mutation of this residue (E3987A) substantially diminishes cytosolic Ca^{2+} sensitivity and increases the EC_{50} of Ca^{2+} activation of [^{3}H]ryanodine binding by ~270-fold[48]. However, unlike the E4872A and E4872Q mutants, single E3987A mutant channels remained sensitive to luminal Ca^{2+} activation, albeit at a reduced sensitivity (**Supplementary Fig. 3**).

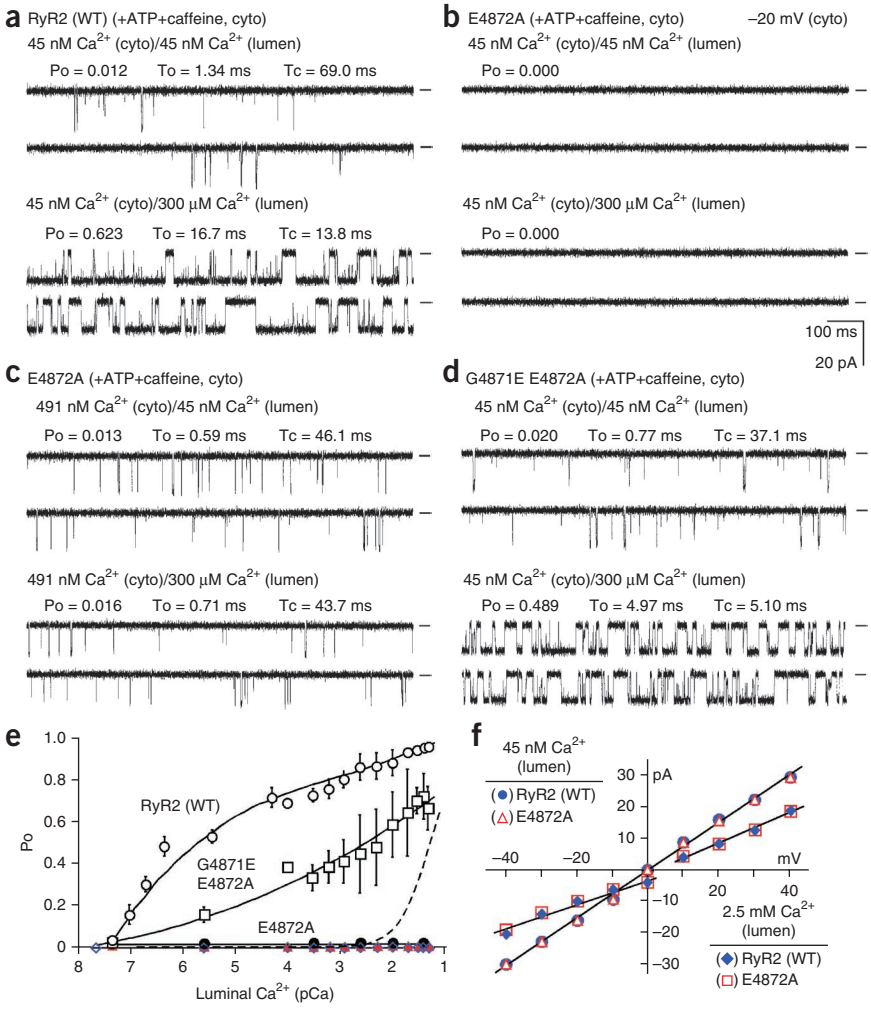

Figure 1 The E4872A mutation abolishes luminal, but not cytosolic, Ca^{2+} activation of RyR2. (**a**–**d**) Single channel activities of WT RyR2 (**a**), E4872A mutant RyR2 (**b**,**c**) and double mutant G4871E E4872A RyR2 (**d**) in the presence of cytosolic (cyto) Ca^{2+} (45 or 491 nM), luminal (lumen) Ca^{2+} (45 or 300 μM), ATP (2.5 mM) and caffeine (2.5 mM). The recording potentials were −20 mV. Zero-current baselines are indicated (short bars). Channel opening is indicated by downward spikes. Also shown are the open probability (Po), mean open time (To) and mean closed time (Tc). (**e**) Po–luminal Ca^{2+} relationships for single WT (white circles; $n = 11$), G4871E E4872A (white squares; $n = 8$) and E4872A (red triangles; $n = 10$) channels with cytosolic Ca^{2+} (45 nM), ATP and caffeine; single E4872A channels with cytosolic Ca^{2+} (491 nM), ATP and caffeine (black circles; $n = 6$); and single E4872A channels with cytosolic Ca^{2+} (45 nM) and ATP but no caffeine (blue diamonds; $n = 6$). The dashed line indicates the response of single WT RyR2 channels to luminal Ca^{2+} in the absence of ATP and caffeine[39]. (**f**) Current-voltage relationships for single WT ($n = 5$) and E4872A mutant ($n = 7$) channels at 45 nM or 2.5 mM luminal Ca^{2+}. The data shown are the mean ± s.e.m.

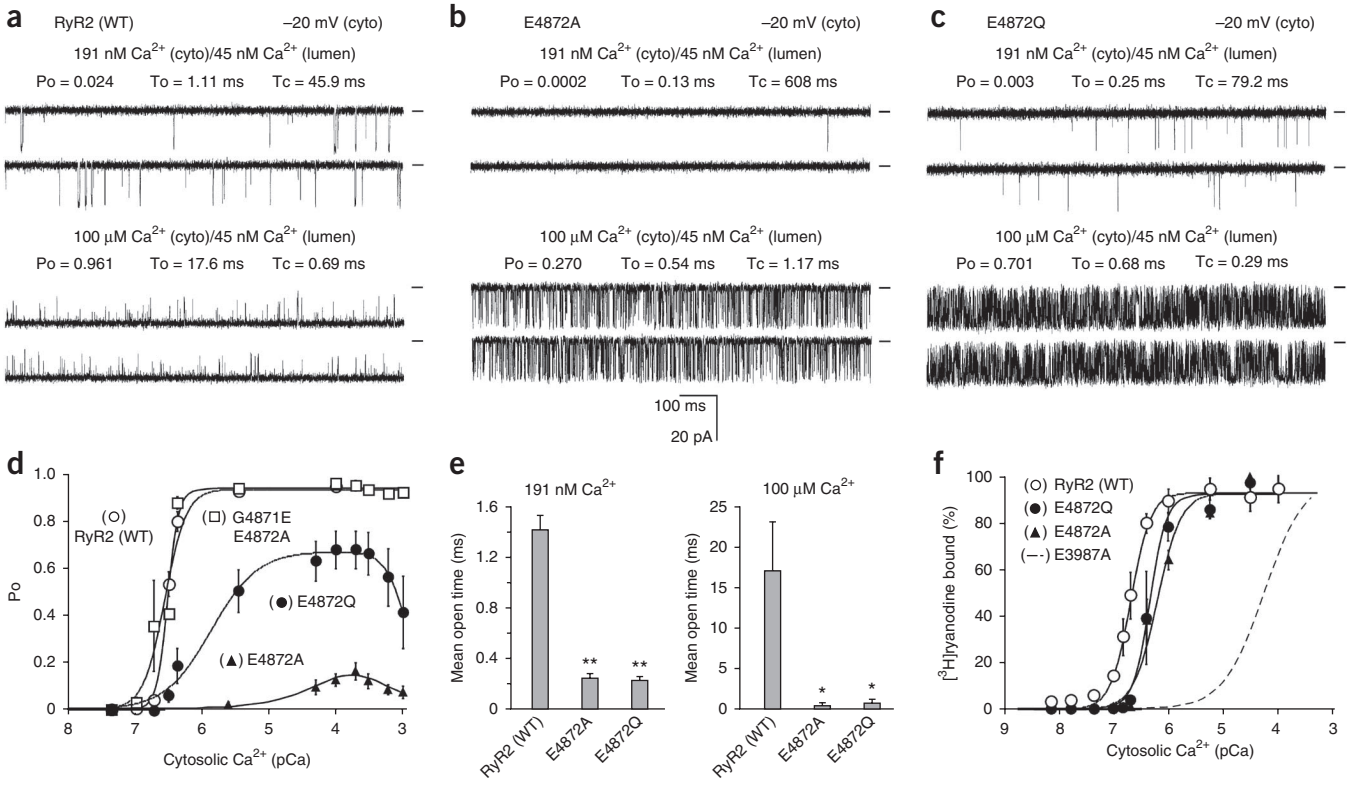

Figure 2 Effects of E4872A and E4872Q on cytosolic Ca^{2+} activation of single RyR2 channels. (**a**–**c**) Single channel activities of WT RyR2 (**a**), E4872A mutant RyR2 (**b**) and E4872Q mutant RyR2 (**c**) recorded in symmetrical recording solutions containing 250 mM KCl and 25 mM 4-(2-hydroxyethyl)-1-piperazineethanesulfonic acid (HEPES) (pH 7.4) in the presence of 191 nM or 100 μM cytosolic Ca^{2+} and 45 nM luminal Ca^{2+}. The recording potentials were –20 mV. Zero-current baselines are indicated (short bars). Channel opening is indicated by downward spikes (**d**) Po–cytosolic Ca^{2+} relationships for single WT ($n = 5$), G4871E E4872A ($n = 4$), E4872Q ($n = 6$) and E4872A ($n = 8$) channels with 45 nM luminal Ca^{2+}. (**e**) Comparison of the mean open time of single WT ($n = 11$), E4872A ($n = 5$) and E4872Q ($n = 8$) channels at 191 nM and the mean open time of single WT ($n = 6$), E4872A ($n = 7$) and E4872Q ($n = 4$) channels at 100 μM cytosolic Ca^{2+} (Student's t test; $^*P < 0.05$, $^{**}P < 0.01$ compared to WT). (**f**) Ca^{2+}-dependent [^{3}H]ryanodine binding to WT ($n = 3$), E4872A ($n = 7$) and E4872Q ($n = 4$) channels. The dashed line represents the binding curve for the cytosolic Ca^{2+} sensor mutant E3987A ($EC_{50} = 59$ μM). The EC_{50} values are 0.22 ± 0.02 μM for WT, 0.72 ± 0.10 μM for E4872A and 0.58 ± 0.12 for E4872Q. The data shown are the mean ± s.e.m.

Therefore, the complete lack of luminal Ca^{2+} response of the E4872A and E4872Q mutants is unlikely to be attributable to their slightly reduced cytosolic Ca^{2+} sensitivity, as luminal Ca^{2+} activation persists even when there is little cytosolic Ca^{2+} sensitivity (as seen for the E3987A channel). Collectively our results demonstrate that the E4872A and E4872Q mutations uniquely and selectively abolish luminal Ca^{2+} sensing and that luminal and cytosolic Ca^{2+} activation processes are different but interactive.

Molecular mechanism of luminal Ca^{2+} sensing

To gain insight into how residue E4872 might be involved in luminal Ca^{2+} sensing, we constructed a model of the RyR2 pore (**Supplementary Fig. 3**) based on the crystal structure of the K^+ channel KcsA[42]. This model is also very similar to the crystal structure of the NaK channel pore (**Supplementary Fig. 4**)[49]. Our model indicates that the E4872 residue lies inside the internal pore, suggesting that luminal Ca^{2+} sensing may take place within the pore. If so, this sensing would require that luminal Ca^{2+} enters the internal pore when the RyR2 is in a closed conformation (**Supplementary Fig. 3**). Electrostatic calculations (**Fig. 3**) predict that the strong negative potential inside the internal pore, when the ion gate of the channel is closed, would be more than sufficient to draw luminal Ca^{2+} through the selectivity filter (i.e., the narrowest part of the channel; **Supplementary Fig. 3**) and into the internal pore. To experimentally explore this possibility, we closed single WT RyR2 channels by reducing cytosolic Ca^{2+} (to 45 nM) in the presence of cytosolic Mg^{2+}. After elevation of luminal Ca^{2+} to 2.5 mM, closed WT, but not E4872A, channels were activated (**Fig. 3a**,**b**). This finding indicates that luminal Ca^{2+} can indeed access the E4872-dependent activation mechanism when the RyR2 is closed. Activation of a closed WT RyR2 by luminal Ca^{2+} persisted even when cytosolic Ca^{2+} was reduced to extremely low levels (0.33 nM or 0.046 nM) (**Supplementary Fig. 5**). This observation is consistent with the notion that luminal Ca^{2+} can control the opening of the RyR2 channel in the absence of cytosolic Ca^{2+} activation.

To determine whether E4872 and/or nearby residues in the helix bundle crossing region (where the inner helices cross each other) interact directly with luminal cations, we used site-directed mutagenesis to manipulate the local cation binding properties of this region. To this end, we generated double histidine RyR2 mutants to create local Ni^{2+} binding sites in this region. We found that one of the mutants, G4871H E4872H, was sensitive to luminal Ni^{2+}. Unlike WT RyR2s, which are insensitive to luminal Ni^{2+} (**Fig. 3c**), closed G4871H E4872H channels were activated by luminal Ni^{2+} (14 nM) (**Fig. 3d**). Thus, luminal Ni^{2+} was able to access and interact with the inserted Ni^{2+} binding site and activate the closed mutant channel.

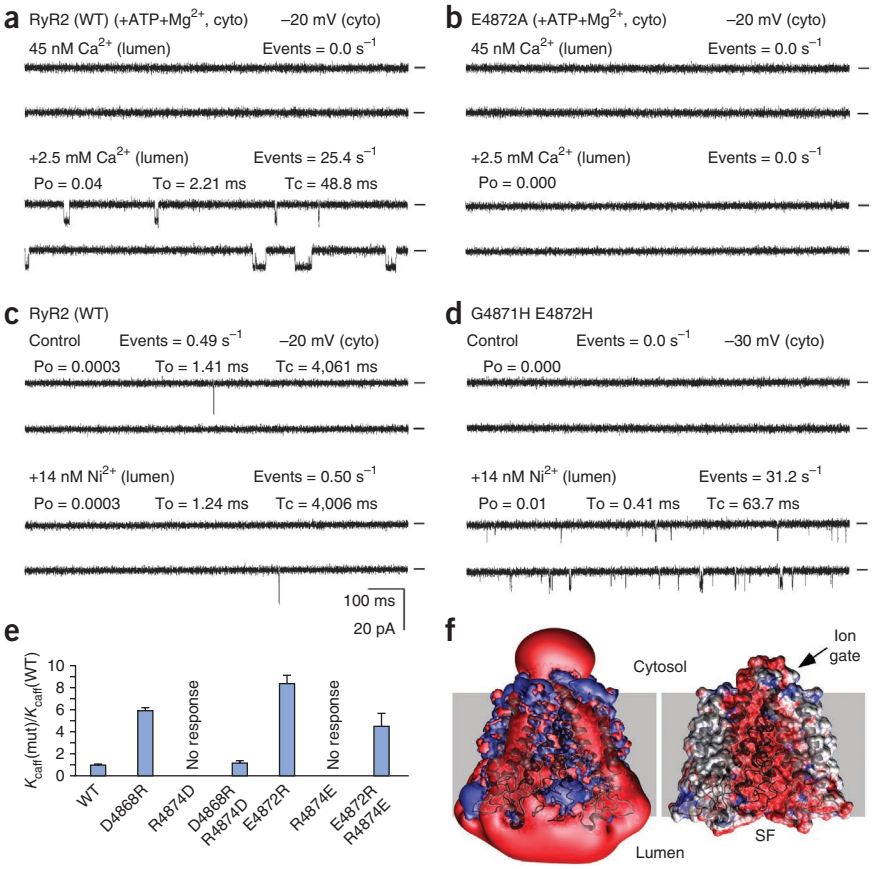

Figure 3 Mechanism of activation of RyR2 by luminal Ca^{2+}. (**a**,**b**) Responses of single WT (**a**) and E4872A mutant (**b**) channels to luminal Ca^{2+} (2.5 mM) in the presence of 45 nM cytosolic Ca^{2+}, 3.0 mM ATP and 1.5 mM Mg^{2+} (1.6 mM free ATP and 0.11 mM free Mg^{2+}). The open event frequency of WT channels increased from 0.02 ± 0.01 to 22 ± 9.0 (mean ± s.e.m.) events per s (n = 5), whereas the open frequency (0.00 events per s) of the E4872A channels did not change (n = 6). (**c**,**d**) Responses of single WT (**c**) and G4871H E4872H (**d**) channels to luminal Ni^{2+} (14 nM) in the presence of 45 nM cytosolic Ca^{2+} and 600 μM luminal Ca^{2+}. The open event frequency of the G4871H E4872H channels increased from 0.03 ± 0.01 to 36 ± 20 events s^{-1} (n = 7), whereas the open frequency of the WT channels did not increase (from 0.40 ± 0.07 to 0.34 ± 0.06 events per s) (n = 5). (**e**) Relative caffeine sensitivities of the indicated single or double mutant channels. The relative caffeine sensitivity for WT and each mutant (mut) channel is defined as the ratio K_{caff}(mut)/K_{caff}(WT), where K_{caff} is the cumulative caffeine concentration that produces 50% of the maximal caffeine-induced Ca^{2+} release. The data shown are the mean ± s.e.m. (n = 3). (**f**) Electrostatic potential isosurface (positive in blue and negative in red) of the RyR2 channel pore model (left) and the electrostatic potential mapped onto a cross-section of the pore (right). SF, selectivity filter.

Further, luminal Ni^{2+} activated closed G4871H E4872H channels even in the presence of extremely low cytosolic Ca^{2+} (0.32 nM or 0.046 nM; **Supplementary Fig. 5**). These results are consistent with the view that cation binding at or near E4872 in the helix bundle crossing region can control the RyR2 gate in the absence of cytosolic Ca^{2+} activation. If the Ni^{2+} ion can access and bind to this site (when the RyR2 is closed), then the smaller-mass Ca^{2+} ion could very well do the same. In other words, the E4872-dependent luminal Ca^{2+}-sensing mechanism may involve a direct interaction of the cation with negative charges in the helix bundle crossing region.

Our model of the RyR2 pore also suggests that the positively charged residue R4874 on one subunit of the RyR2 tetramer likely interacts with either or both of the negatively charged residues D4868 and E4872 on the neighboring subunit (**Supplementary Fig. 3**). To experimentally test this possibility, we reversed the charge polarity of these individual residues by generating channels with the single mutations D4868R, E4872R, R4874D or R4874E. Each of these single mutations markedly reduced or abolished RyR2 function (**Fig. 3e** and **Supplementary Fig. 5**). We also generated double mutants in which we changed the positively charged residue to a negatively charged residue and the potentially interacting negatively charged partner to a positively charged residue (D4868R R4874D and E4872R R4874E). Notably, the D4868R R4874D double mutation largely and the E4872R R4874E mutation partially restored caffeine responsiveness (**Fig. 3e** and **Supplementary Fig. 5**). The observation that the E4872R R4874E mutation only partially restores caffeine responsiveness may be related to the involvement of the E4872 residue in both electrostatic interactions and luminal Ca^{2+} sensing. To determine whether the electrostatic interaction between D4868 and E4872 is intrasubunit or intersubunit, we coexpressed channels with each of two single mutations (D4868R and R4874D or E4872R and R4874E) to produce heterotetrameric RyR2s containing both types of mutant subunits. Coexpression of the pairs of mutant channels restored caffeine responsiveness (**Supplementary Fig. 5**), indicating that the electrostatic interactions are between residues on neighboring subunits (i.e., intersubunit interactions), as predicted by our model (**Supplementary Fig. 3**). These data also demonstrate that local electrostatic interactions exist within the helix bundle crossing region (the putative RyR2 gate). By virtue of their electrostatic interactions, residues D4868 and R4874 may have a vital role in stabilizing the helix bundle crossing region and thus the operation of the RyR2 gate. Residue E4872, which is essential for luminal Ca^{2+} sensing, is also involved in these electrostatic interactions. Therefore, we propose that the RyR2 helix bundle crossing region encompasses a store Ca^{2+}-sensing gate, as it contains structural elements that are critical for both luminal Ca^{2+} sensing and channel gating. Notably, residues D4868, E4872 and R4874 are conserved in all RyR and IP3R isoforms (**Supplementary Fig. 6**), implying that this store-sensing gate structure may be a common feature of Ca^{2+} release channels.

Residue E4872 is a critical determinant of Ca^{2+} waves

In the next series of experiments, we assessed the role of this RyR2 store-sensing gate in store overload-induced Ca^{2+} oscillations or Ca^{2+} waves (i.e., SOICR). Unlike HEK293 cells expressing the WT channel, HEK293 cells expressing the E4872A or E4872Q mutant channel displayed little or no SOICR (**Fig. 4a–c**). In HL-1 mouse cardiac cells, expression of either the E4872A or E4872Q mutant channel, but not the WT channel, essentially abolished SOICR (**Fig. 4d** and **Supplementary Fig. 6**). Because the GFP-tagged E4872A and E4872Q mutants were overexpressed in HL-1 cells, most, if not all,

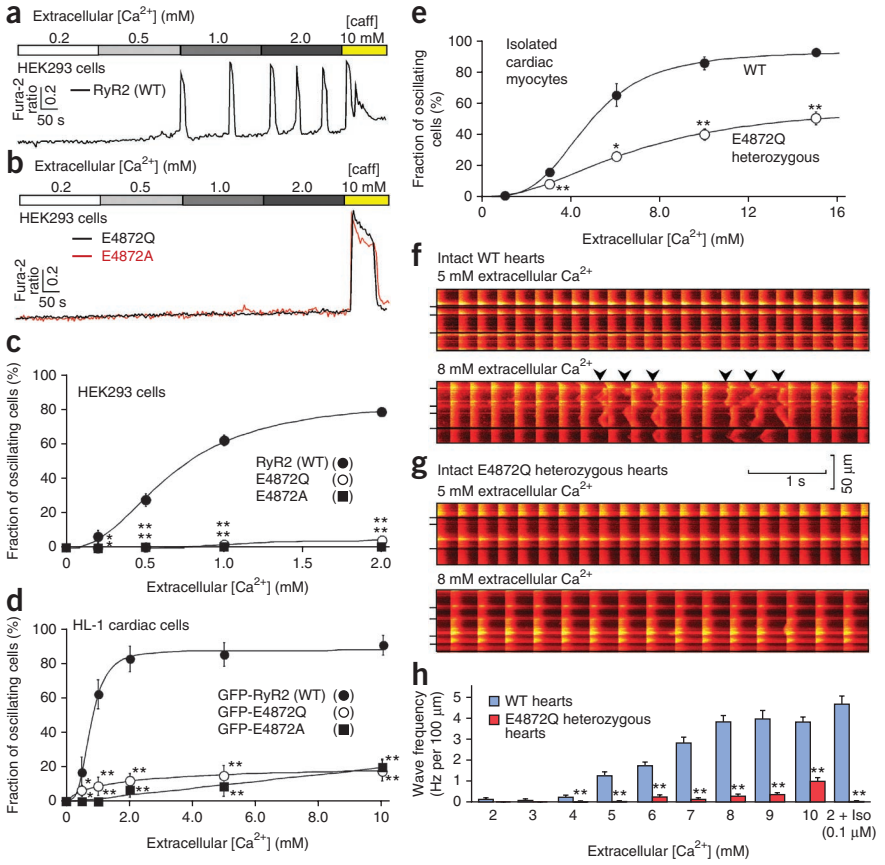

Figure 4 Effect of E4872 mutations on SOICR. (**a**,**b**) Cytosolic Ca^{2+} dynamics in HEK293 cells expressing WT RyR2 (**a**) or either E4872Q or E4872A mutant RyR2 (**b**), perfused with increasing levels of extracellular Ca^{2+} (overloading the Ca^{2+} store and triggering SOICR). (**c**) The percentage of HEK293 cells expressing WT RyR2 (523, the total number of cells in each group), E4872Q RyR2 (674) or E4872A RyR2 (337) that displayed Ca^{2+} oscillations ($n = 4$). (**d**) The percentage of HL-1 cells transfected with GFP-tagged WT RyR2 (25 cells), GFP-tagged E4872Q RyR2 (33 cells) or GFP-tagged E4872A RyR2 (65 cells) that displayed Ca^{2+} oscillations ($n = 6$). (**e**) The percentage of isolated ventricular myocytes from WT (445 cells) ($n = 14$ mice) or heterozygous E4872Q mice (506 cells) ($n = 15$ mice) that displayed SOICR. (**f**,**g**) *In situ* line-scan confocal imaging of Ca^{2+} transients in intact hearts from WT (**f**) and heterozygous E4872Q (**g**) mice perfused with 5 or 8 mM extracellular Ca^{2+}. Arrowheads indicate the occurrence of spontaneous Ca^{2+} waves. Short bars on the left indicate cell boundaries. (**h**) Ca^{2+} wave frequency in ventricular myocytes in intact hearts from WT ($n = 4$) or heterozygous E4872Q mutant ($n = 3$) mice at the indicated extracellular Ca^{2+} concentrations (2–10 mM) with or without 0.1 μM isoproterenol (Iso). The data shown are the mean ± s.e.m. from 40–100 images (Student's *t* test; $*P < 0.05$, $**P < 0.01$ compared to WT).

endogenous WT RyR2 subunits would form heteromeric channels with GFP-tagged mutant subunits. Thus, the E4872A and E4872Q mutant channels probably exert their negative effect on SOICR in the presence of endogenous WT RyR2 through formation of WT-mutant heteromeric channels. Thus, the E4872 residue that is essential for luminal Ca^{2+} activation of RyR2 is also critical for SOICR.

We next explored the importance of the RyR2 store-sensing gate in the context of adult cardiomyocytes and intact hearts by generating a knock-in mouse strain that harbors the RyR2 E4872Q mutation (**Supplementary Fig. 6**). We chose the isosteric E4872Q mutation because it is a slightly more conservative amino acid substitution than is E4872A and would thus be likely to produce a less-severe phenotype, as suggested by our single-channel studies (**Fig. 2d** and **Supplementary Fig. 2**). Heterozygous E4872Q mutant embryos survived, and heterozygous E4872Q adult mice had no gross structural or functional abnormalities detectable by echocardiography (**Supplementary Table 1**). However, homozygous E4872Q mutation was embryonically lethal, with most embryos dying between embryonic days 10.5 and 11.5 (**Supplementary Fig. 6**), indicating that E4872-based RyR2 luminal Ca^{2+} regulation is important for normal embryonic development.

Cardiomyocytes isolated from heterozygous E4872Q mice had a reduced propensity for SOICR compared to WT cells (**Fig. 4e** and **Supplementary Fig. 7**). We also determined the SOICR propensity in the ventricles of intact WT and mutant hearts *ex vivo* using line-scan confocal imaging. Elevation of extracellular Ca^{2+} (to 2–10 mM) or application of isoproterenol increased the frequency of spontaneous Ca^{2+} waves in intact WT hearts (**Fig. 4f**,**h**). However, the same experimental maneuvers resulted in very few or no Ca^{2+} waves in intact heterozygous E4872Q hearts (**Fig. 4g**,**h**). Thus, the E4872-dependent luminal Ca^{2+}-sensing mechanism determines the likelihood of SOICR in HEK293 cells, HL-1 cardiac cells, freshly isolated cardiomyocytes and intact hearts.

Impact of E4872Q on excitation-contraction coupling

To determine whether the E4872Q mutation affects normal cardiac excitation-contraction (EC) coupling, we examined depolarization- and caffeine-induced intracellular Ca^{2+} transients. We found no statistically significant differences in the amplitude of depolarization-induced Ca^{2+} transients (**Fig. 5a–f**), resting cytosolic Ca^{2+} concentration or SR Ca^{2+} content (**Fig. 5c**) between WT and E4872Q cardiomyocytes when 1.8 mM extracellular Ca^{2+} was present. However, SR Ca^{2+} content was significantly greater in E4872Q heterozygous cardiomyocytes than in WT control cells when bathed at 5 mM extracellular Ca^{2+} (to overload the SR) (**Supplementary Fig. 7**). This is probably because as the Ca^{2+} load increased, leak through E4872Q subunit-containing RyR2s was suppressed compared to that through WT RyR2, resulting in a higher SR Ca^{2+} load. Thus, the E4872Q mutation in a heterozygous state suppresses SOICR and increases SR Ca^{2+} content under conditions of SR Ca^{2+} overload, but does not markedly affect SR Ca^{2+} content under nonoverload conditions.

The L-type Ca^{2+} channel current in E4872Q cardiomyocytes was significantly increased compared to that in WT cells (**Fig. 5g**), resulting in a reduced EC coupling gain (**Fig. 5h**). Furthermore, the time to the peak of the Ca^{2+} transient was significantly increased in E4872Q compared to WT cardiomyocytes, whereas late decay times (T_{75} (time from peak to 75% decay in the Ca^{2+} transient) and T_{90} (but not T_{50}) were significantly shorter (**Fig. 5i** and **Supplementary Fig. 7**).

While the exact reasons for the faster late decay times in E4872Q cardiomyocytes are unclear, they may be due in part to enhanced

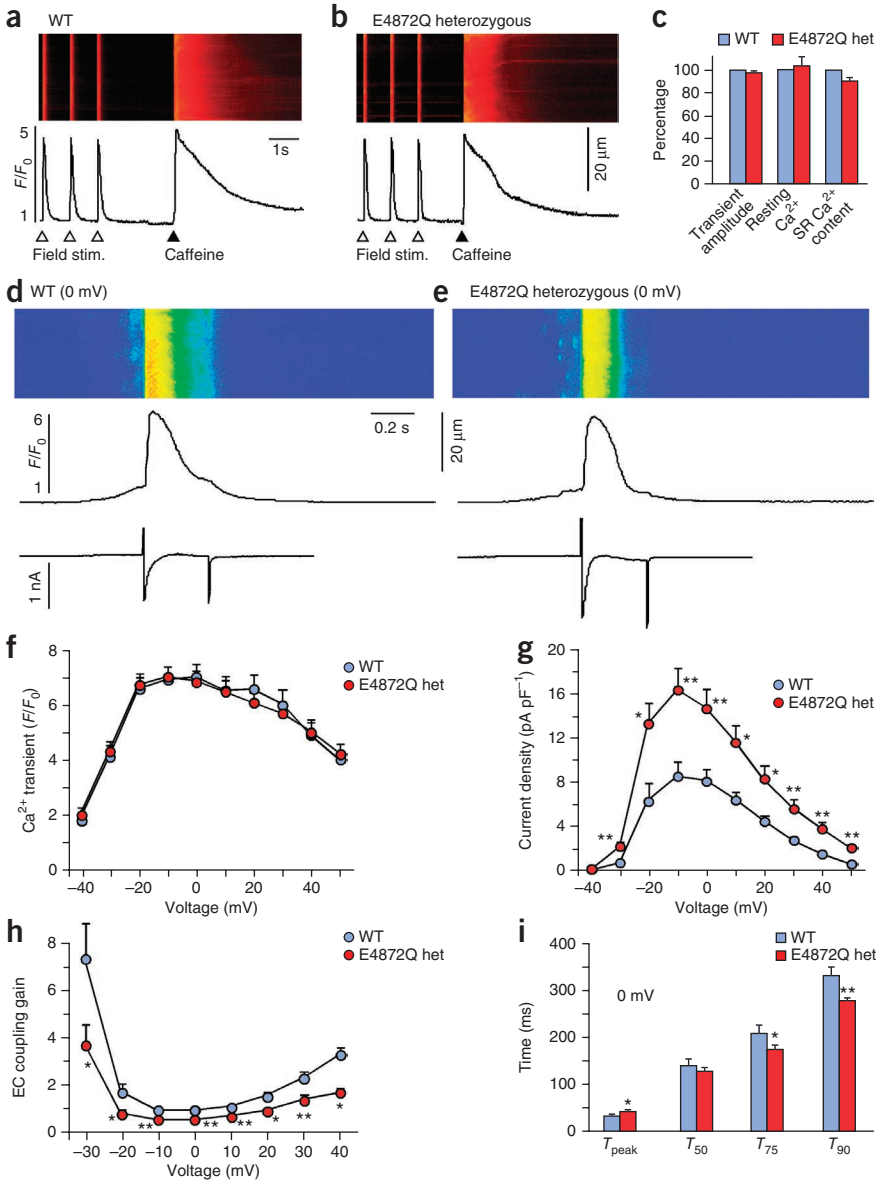

Figure 5 Effect of the E4872Q RyR2 mutation on EC coupling. (**a**,**b**) Line-scan confocal imaging of field-stimulated (stim.) and caffeine-induced Ca^{2+} transients in isolated WT (**a**) and heterozygous E4872Q (**b**) ventricular myocytes loaded with Rhod-2 AM. (**c**) Field-stimulated Ca^{2+} transient amplitudes, resting Ca^{2+} levels and caffeine-induced Ca^{2+} release (SR Ca^{2+} content) in WT ($n = 37$) and E4872Q heterozygous (het; $n = 47$) myocytes. The data shown are the mean ± s.e.m. (**d**,**e**) Simultaneous recordings of depolarization (0 mV)-induced Ca^{2+} transients and L-type Ca^{2+} current ($I_{Ca,L}$) in isolated WT (**d**) and E4872Q (**e**) myocytes (holding potential, −80 mV). (**f**–**i**) Depolarization-induced Ca^{2+} transient amplitude (**f**), $I_{Ca,L}$ current density (**g**), EC coupling gain (**h**) and the kinetics of the Ca^{2+} transient (at 0 mV) (**i**) in WT and heterozygous E4872Q ventricular myocytes (T_{peak}, time to peak; T_{50}, T_{75} and T_{90}, time from peak to 50%, 75% and 90% decay in the Ca^{2+} transient, respectively). Depolarization was from −40 to 50 mV. The data shown are the mean ± s.e.m. from 14 WT and 17 E4872Q cells (Student's *t* test; $^*P < 0.05$, $^{**}P < 0.01$ compared to WT).

Na^+-Ca^{2+} exchanger activity (**Supplementary Fig. 7**). In contrast, the rate of decay of caffeine-induced Ca^{2+} transients in WT RyR2 and E4872Q heterozygous mutant cardiomyocytes was not significantly different (**Supplementary Fig. 8**). The shorter open time and reduced Ca^{2+} sensitivity of the E4872Q mutant channel would be expected to decrease the rate of SR Ca^{2+} release and caffeine-induced SR Ca^{2+} store depletion and thus slow the decay of caffeine-induced Ca^{2+} transients. Conversely, enhanced Na^+-Ca^{2+} exchanger activity in E4872Q heterozygous cardiomyocytes would speed up the decay of caffeine-induced Ca^{2+} transients. These opposite effects may account for the unchanged decay time of caffeine-induced Ca^{2+} transients.

Overall, our results indicate that the E4872Q mutation desensitizes RyR2 to normal Ca^{2+}-induced Ca^{2+} release. This desensitization may be related to the shorter open times and decreased cytosolic Ca^{2+} sensitivity of E4872Q mutant channels (**Fig. 2d**–**f**). In turn, this desensitization would promote a compensatory increase in systolic Ca^{2+} influx (**Fig. 5g**) and diastolic Ca^{2+} extrusion (**Supplementary Fig. 7**) that helps normalize the amplitude of Ca^{2+} transients.

E4872Q completely protects against stress-induced VTs

We previously showed that the RyR2 R4496C mutation associated with catecholaminergic polymorphic ventricular tachycardia (CPVT) in humans enhances SOICR[14]. In RyR2 R4496C knock-in mice, CPVT was readily induced by the administration of caffeine and epinephrine (**Fig. 6a**)[50]. To determine whether the E4872Q mutation is able to prevent CPVT, we generated a compound mutant mouse strain (R4496C E4872Q) in which one RyR2 allele harbors the R4496C mutation and the other the E4872Q mutation. R4496C E4872Q mice were completely resistant to CPVT induction (**Fig. 6b**–**d**).

To assess the expression of WT and E4872Q RyR2 in E4872Q heterozygous hearts, we performed reverse transcription (RT)-PCR, direct DNA sequencing analysis and immunoblotting analysis. We isolated heart mRNA and amplified a fragment of the RyR2 mRNA containing the E4872Q mutation using RT-PCR. We subcloned this fragment into the pBluescript plasmid and isolated 103 clones. Direct DNA sequencing of these clones revealed that 59 of the 103 clones (57.3%) corresponded to E4872Q mutant RyR2 and 44 of the 103 clones (42.7%) to WT RyR2. We carried out similar studies with R4496C E4872Q compound heterozygous mutant hearts. Direct DNA sequencing analysis revealed that 52 of the 105 clones (49.5%) corresponded to the R4496C mutant allele and 53 of the 105 clones (50.5%) to the E4872Q mutant allele. We also determined total RyR2 protein levels in WT and E4872Q heterozygous mutant hearts by immunoblotting. Consistent with the mRNA study, we found that the RyR2 protein levels in WT and E4872Q heterozygous mutant hearts were not significantly different (**Supplementary Fig. 8**). We also assessed the expression levels of SERCA2a (also known as ATP2A2), CASQ2, triadin and junctin in WT and E4872Q heterozygous hearts, and found

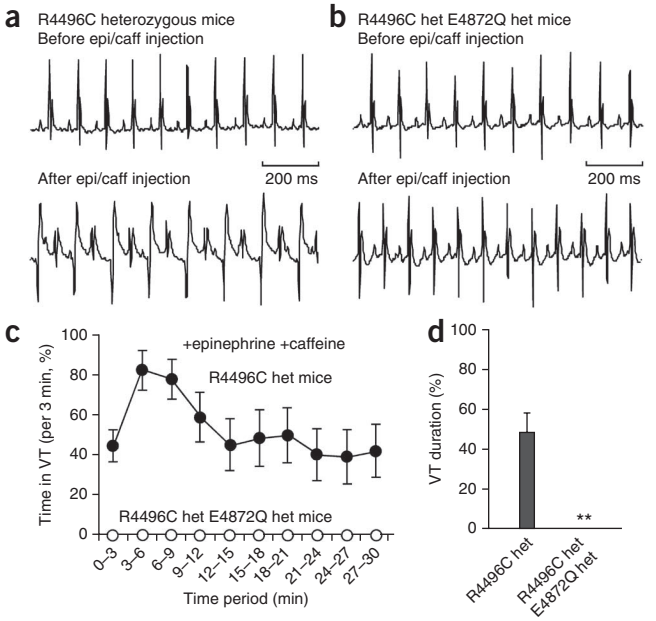

Figure 6 Heterozygous E4872Q mutant mice are resistant to SOICR-induced VTs. (**a**,**b**) Representative electrocardiogram (ECG) recordings of heterozygous R4496C (**a**) and compound heterozygous R4496C E4872Q (**b**) mutant mice before and after injection of epinephrine (1.6 mg per kg body weight) and caffeine (120 mg per kg body weight). Epi/caff, epinephrine and caffeine. (**c**,**d**) VT duration (%) in heterozygous R4496C ($n = 7$) and compound heterozygous R4496C E4872Q ($n = 7$) mice within each indicated 3-min (**c**) or 30-min (**d**) period of ECG recording (Student's t test; $P < 0.05$ for all points as compared to R4496C). The data shown are the mean ± s.e.m.

no significant differences in their expression levels (**Supplementary Fig. 8**). Thus, the phenotypes we observed in the E4872Q heterozygous and R4496C E4872Q compound heterozygous mutant hearts are unlikely to be due to altered expression of RyR2 and its associated proteins (CASQ2, triadin and junctin). Because VTs in RyR2 R4496C mutant mice are caused by triggered activities induced by spontaneous Ca^{2+} waves[27,50–52], it seems reasonable to propose that the E4872Q mutation prevents VTs by suppressing the occurrence of spontaneous Ca^{2+} waves.

DISCUSSION

Spontaneous Ca^{2+} release during SOICR has long been observed in cardiac cells[3,18–22]. This SOICR occurs as a result of RyR2 opening when store Ca^{2+} content exceeds a threshold level[10,13,30,31], but the molecular mechanism responsible for this has been a longstanding mystery. Here we demonstrate that the helix bundle crossing region of RyR2 (its proposed gate) encompasses an essential component of the store (luminal) Ca^{2+}-sensing mechanism that controls SOICR and thus Ca^{2+}-triggered VTs. This store Ca^{2+}-sensing gate also governs normal luminal Ca^{2+} regulation of RyR2 and EC coupling gain. Thus, this store Ca^{2+}-sensing mechanism has an important role in both normal physiology and disease.

Our results demonstrate that the E4872 residue located in the helix bundle crossing region is essential for luminal Ca^{2+} activation of RyR2. However, it is unlikely that E4872 is the only residue involved in the luminal Ca^{2+}-sensing mechanism, as Ca^{2+} binding often involves ion coordination with multiple oxygen donors that form a Ca^{2+}-binding pocket. Identification and characterization of all the residues involved in the formation of the luminal Ca^{2+}-binding pocket will be a daunting task, but our discovery that E4872 is an essential element is an important first step toward understanding the underlying mechanism.

Besides its essential role in luminal Ca^{2+} sensing, the E4872 residue is also part of a network of intersubunit salt bridges within the RyR2 helix bundle crossing region, the proposed gate of RyR2. We propose that when luminal Ca^{2+} associates with E4872, intersubunit electrostatic interactions between residues D4868, E4872 and R4874 are disrupted, thereby increasing the likelihood that the channel transitions from the closed to the open state. Additional studies will be required to verify this working model of how luminal Ca^{2+} controls RyR2 gating.

The E4872Q mutation completely abolishes luminal Ca^{2+} activation of RyR2 despite the presence of luminal-to-cytosolic Ca^{2+} flux and cytosolic Ca^{2+} activation, albeit with a reduced sensitivity. Conversely, the E3987A mutant channel, which exhibits a markedly diminished cytosolic Ca^{2+} response[48], remains responsive to luminal Ca^{2+} activation. Furthermore, luminal Ca^{2+} (or luminal Ni^{2+}) is able to open a closed single WT (or G4871H E4872H mutant) RyR2 channel in the absence of cytosolic Ca^{2+} activation. Taken together, these observations indicate that luminal and cytosolic Ca^{2+} activation of RyR2 are mediated by different but interacting mechanisms, consistent with earlier observations[53,54]. Cytosolic Ca^{2+} activation of RyR2 involves a cytosolic Ca^{2+} sensor[48], whereas luminal Ca^{2+} activation of RyR2 clearly involves a luminal Ca^{2+} sensor. However, luminal and cytosolic Ca^{2+} activation of RyR2 are inherently interactive because both of these Ca^{2+} sensors govern the same gate.

Pharmacological agents that reduce RyR2 open time suppress Ca^{2+} waves and Ca^{2+}-triggered VTs[50,55,56]. Interestingly, the E4872Q mutation also reduced the duration of RyR2 opening, decreased the likelihood of SOICR and completely suppressed VTs in CPVT-prone mouse hearts. Thus, limiting RyR2 open time seems to be a common and effective means of suppressing Ca^{2+}-mediated arrhythmias. Thus, we propose that the RyR2 store Ca^{2+}-sensing gate could represent a potential therapeutic target for anti-arrhythmic therapies.

While luminal Ca^{2+} regulation of RyR2 by the CASQ2 protein is well established[17,36], the E4872-based luminal Ca^{2+} sensing mechanism defined here does not require CASQ2. In our single channel and cell-line studies, the E4872A and E4872Q mutations altered RyR2 luminal Ca^{2+} regulation in the absence of CASQ2. Even when CASQ2 was present, as in our cardiomyocyte and intact heart studies, the E4872A and E4872Q mutations substantially altered RyR2 luminal Ca^{2+} sensing. Although the relationship between the E4872- and CASQ2-based luminal Ca^{2+} sensing mechanisms is not yet entirely clear, our results show that the E4872-based mechanism can operate in the absence of CASQ2. This mechanism may explain why SR Ca^{2+} release is still governed by luminal Ca^{2+} in CASQ2-null mouse cardiomyocytes[37].

The amino acid sequence surrounding the RyR2 E4872 residue is completely conserved in all three mammalian RyR isoforms across different species, implying that all RyR isoforms have the same store Ca^{2+}-sensing gate structure. This inference is consistent with the reported luminal Ca^{2+} sensitivity of single skeletal muscle RyR channels (RyR1)[32,57], as well as with SR Ca^{2+} load–dependent spontaneous Ca^{2+} release in isolated skeletal muscle SR vesicles[53] and skeletal muscle fibers[58]. Spontaneous Ca^{2+} release during SR Ca^{2+} overload has also been observed in RyR3-containing smooth muscle cells[59]. The key RyR2 residues (D4868, E4872 and R4874) involved in store Ca^{2+} sensing are also conserved in all IP3R isoforms, raising the intriguing

possibility that IP3R luminal Ca^{2+} sensitivity[5–8] may also be governed by a store-sensing gate.

METHODS

Methods and any associated references are available in the online version of the paper.

Note: Any Supplementary Information and Source Data files are available in the online version of the paper.

ACKNOWLEDGMENTS

This work was supported by research grants from the Canadian Institutes of Health Research (CIHR) to H.J.D., D.P.T. and S.R.W.C., the US National Institutes of Health to J.C., L.-S.S., M.F. and S.R.W.C., the Heart and Stroke Foundation of Alberta to A.M.G., H.J.D. and S.R.W.C. and the Canada Foundation for Innovation (S.R.W.C.) and by the Heart and Stroke Foundation/Libin Cardiovascular Institute Professorship in Cardiovascular Research (S.R.W.C.). We are grateful for generous donations from the King family, the Howarth family and the Libin Cardiovascular Institute of Alberta. We are also grateful to W.C. Claycomb from the Louisiana State University Health Sciences Center for kindly providing the HL-1 cardiac cell line and to J. Lytton from the University of Calgary for the gift of the β-actin–specific antibody. W.C., X.Z. and X.T. are recipients of the Alberta Innovates-Health Solutions (AIHS) Studentship Award; P.P.J. is a recipient of AIHS and Heart and Stroke Foundation Fellowship Awards; M.L.O. is the recipient of a CIHR Fellowship Award; and H.J.D., D.P.T. and S.R.W.C. are recipients of AIHS Scientist Awards.

AUTHOR CONTRIBUTIONS

W.C., R.W., B.C., X.Z., H.K., Y.B., Q.Z., A.G., X.T., P.P.J., M.L.O., J.C., D.P.T., A.M.G., H.J.D., M.F., L.-S.S. and S.R.W.C. designed research. W.C., R.W., B.C., X.Z., H.K., Y.B., Q.Z., C.X., Jingqun Zhang, A.G., X.T., P.P.J., M.L.O., Y.L., T.M., L.Z., J.B., L.S., H.C. and Jianlin Zhang performed research. W.C., R.W., Y.B., X.Z., H.K., Y.B., Q.Z., C.X., Jingqun Zhang, A.G., X.T., P.P.J., M.L.O., Y.L., T.M., L.Z., J.B., Jianlin Zhang, L.-S.S. and S.R.W.C. analyzed data. W.C., X.Z., Y.B., P.P.J., M.L.O., M.F., L.-S.S. and S.R.W.C. wrote the paper.

COMPETING FINANCIAL INTERESTS

The authors declare no competing financial interests.

1. Bers, D.M. Cardiac excitation-contraction coupling. *Nature* **415**, 198–205 (2002).
2. Berridge, M.J., Bootman, M.D. & Roderick, H.L. Calcium signalling: dynamics, homeostasis and remodelling. *Nat. Rev. Mol. Cell Biol.* **4**, 517–529 (2003).
3. Fabiato, A. Time and calcium dependence of activation and inactivation of calcium-induced release of calcium from the sarcoplasmic reticulum of a skinned canine cardiac Purkinje cell. *J. Gen. Physiol.* **85**, 247–289 (1985).
4. Bers, D.M. Calcium cycling and signaling in cardiac myocytes. *Annu. Rev. Physiol.* **70**, 23–49 (2008).
5. Irvine, R.F. 'Quantal' Ca^{2+} release and the control of Ca^{2+} entry by inositol phosphates—a possible mechanism. *FEBS Lett.* **263**, 5–9 (1990).
6. Missiaen, L., Taylor, C.W. & Berridge, M.J. Spontaneous calcium release from inositol trisphosphate-sensitive calcium stores. *Nature* **352**, 241–244 (1991).
7. Missiaen, L., Taylor, C.W. & Berridge, M.J. Luminal Ca^{2+} promoting spontaneous Ca^{2+} release from inositol trisphosphate-sensitive stores in rat hepatocytes. *J. Physiol. (Lond.)* **455**, 623–640 (1992).
8. Nunn, D.L. & Taylor, C.W. Luminal Ca^{2+} increases the sensitivity of Ca^{2+} stores to inositol 1,4,5-trisphosphate. *Mol. Pharmacol.* **41**, 115–119 (1992).
9. Sitsapesan, R. & Williams, A. Regulation of the gating of the sheep cardiac sarcoplasmic reticulum Ca^{2+}-release channel by luminal Ca^{2+}. *J. Membr. Biol.* **137**, 215–226 (1994).
10. Bassani, J.W., Yuan, W., Bers, D.M. & Fractional, S.R. Ca release is regulated by trigger Ca and SR Ca content in cardiac myocytes. *Am. J. Physiol.* **268**, C1313–C1319 (1995).
11. Györke, I. & Gyorke, S. Regulation of the cardiac ryanodine receptor channel by luminal Ca^{2+} involves luminal Ca^{2+} sensing sites. *Biophys. J.* **75**, 2801–2810 (1998).
12. Xu, L. & Meissner, G. Regulation of cardiac muscle Ca^{2+} release channel by sarcoplasmic reticulum lumenal Ca^{2+}. *Biophys. J.* **75**, 2302–2312 (1998).
13. Shannon, T.R., Ginsburg, K.S. & Bers, D.M. Potentiation of fractional sarcoplasmic reticulum calcium release by total and free intra-sarcoplasmic reticulum calcium concentration. *Biophys. J.* **78**, 334–343 (2000).
14. Jiang, D. *et al.* RyR2 mutations linked to ventricular tachycardia and sudden death reduce the threshold for store-overload–induced Ca^{2+} release (SOICR). *Proc. Natl. Acad. Sci. USA* **101**, 13062–13067 (2004).
15. Keller, M., Kao, J.P., Egger, M. & Niggli, E. Calcium waves driven by "sensitization" wave-fronts. *Cardiovasc. Res.* **74**, 39–45 (2007).
16. Kong, H. *et al.* Skeletal and cardiac ryanodine receptors exhibit different responses to Ca^{2+} overload and luminal Ca^{2+}. *Biophys. J.* **92**, 2757–2770 (2007).
17. Györke, S. & Terentyev, D. Modulation of ryanodine receptor by luminal calcium and accessory proteins in health and cardiac disease. *Cardiovasc. Res.* **77**, 245–255 (2008).
18. Kass, R.S. & Tsien, R.W. Fluctuations in membrane current driven by intracellular calcium in cardiac Purkinje fibers. *Biophys. J.* **38**, 259–269 (1982).
19. Orchard, C.H., Eisner, D. & Allen, D. Oscillations of intracellular Ca^{2+} in mammalian cardiac muscle. *Nature* **304**, 735–738 (1983).
20. Stern, M.D., Kort, A., Bhatnagar, G. & Lakatta, E. Scattered-light intensity fluctuations in diastolic rat cardiac muscle caused by spontaneous Ca^{2+}-dependent cellular mechanical oscillations. *J. Gen. Physiol.* **82**, 119–153 (1983).
21. Wier, W.G., Kort, A., Stern, M., Lakatta, E. & Marban, E. Cellular calcium fluctuations in mammalian heart: direct evidence from noise analysis of aequorin signals in Purkinje fibers. *Proc. Natl. Acad. Sci. USA* **80**, 7367–7371 (1983).
22. Marban, E., Robinson, S.W. & Wier, W.G. Mechanisms of arrhythmogenic delayed and early afterdepolarizations in ferret ventricular muscle. *J. Clin. Invest.* **78**, 1185–1192 (1986).
23. Schlotthauer, K. & Bers, D.M. Sarcoplasmic reticulum Ca^{2+} release causes myocyte depolarization. Underlying mechanism and threshold for triggered action potentials. *Circ. Res.* **87**, 774–780 (2000).
24. Bers, D.M. Calcium and cardiac rhythms: physiological and pathophysiological. *Circ. Res.* **90**, 14–17 (2002).
25. Pogwizd, S.M. & Bers, D.M. Cellular basis of triggered arrhythmias in heart failure. *Trends Cardiovasc. Med.* **14**, 61–66 (2004).
26. Jiang, D. *et al.* Enhanced store overload–induced Ca^{2+} release and channel sensitivity to luminal Ca^{2+} activation are common defects of RyR2 mutations linked to ventricular tachycardia and sudden death. *Circ. Res.* **97**, 1173–1181 (2005).
27. Priori, S.G. & Chen, S.R. Inherited dysfunction of sarcoplasmic reticulum Ca^{2+} handling and arrhythmogenesis. *Circ. Res.* **108**, 871–883 (2011).
28. Nelson, M.T. *et al.* Relaxation of arterial smooth muscle by calcium sparks. *Science* **270**, 633–637 (1995).
29. Lakatta, E.G., Maltsev, V.A. & Vinogradova, T.M. A coupled system of intracellular Ca^{2+} clocks and surface membrane voltage clocks controls the timekeeping mechanism of the heart's pacemaker. *Circ. Res.* **106**, 659–673 (2010).
30. Díaz, M.E., Trafford, A.W., O'Neill, S.C. & Eisner, D.A. Measurement of sarcoplasmic reticulum Ca^{2+} content and sarcolemmal Ca^{2+} fluxes in isolated rat ventricular myocytes during spontaneous Ca^{2+} release. *J. Physiol. (Lond.)* **501**, 3–16 (1997).
31. Eisner, D.A., Kashimura, T., Venetucci, L.A. & Trafford, A.W. From the ryanodine receptor to cardiac arrhythmias. *Circ. J.* **73**, 1561–1567 (2009).
32. Tripathy, A. & Meissner, G. Sarcoplasmic reticulum lumenal Ca^{2+} has access to cytosolic activation and inactivation sites of skeletal muscle Ca^{2+} release channel. *Biophys. J.* **70**, 2600–2615 (1996).
33. Jiang, D., Chen, W., Wang, R., Zhang, L. & Chen, S.R.W. Loss of luminal Ca^{2+} activation in the cardiac ryanodine receptor is associated with ventricular fibrillation and sudden death. *Proc. Natl. Acad. Sci. USA* **104**, 18309–18314 (2007).
34. Laver, D.R. Ca^{2+} stores regulate ryanodine receptor Ca^{2+} release channels via luminal and cytosolic Ca^{2+} sites. *Biophys. J.* **92**, 3541–3555 (2007).
35. Liu, Y. *et al.* Flux regulation of cardiac ryanodine receptor channels. *J. Gen. Physiol.* **135**, 15–27 (2010).
36. Györke, I., Hester, N., Jones, L.R. & Gyorke, S. The role of calsequestrin, triadin, and junctin in conferring cardiac ryanodine receptor responsiveness to luminal calcium. *Biophys. J.* **86**, 2121–2128 (2004).
37. Knollmann, B.C. *et al.* Casq2 deletion causes sarcoplasmic reticulum volume increase, premature Ca^{2+} release, and catecholaminergic polymorphic ventricular tachycardia. *J. Clin. Invest.* **116**, 2510–2520 (2006).
38. Sitsapesan, R. & Williams, A.J. Regulation of current flow through ryanodine receptors by luminal Ca^{2+}. *J. Membr. Biol.* **159**, 179–185 (1997).
39. Kong, H. *et al.* Caffeine induces Ca^{2+} release by reducing the threshold for luminal Ca^{2+} activation of the ryanodine receptor. *Biochem. J.* **414**, 441–452 (2008).
40. Zhao, M. *et al.* Molecular identification of the ryanodine receptor pore-forming segment. *J. Biol. Chem.* **274**, 25971–25974 (1999).
41. Williams, A.J., West, D.J. & Sitsapesan, R. Light at the end of the Ca^{2+}-release channel tunnel: structures and mechanisms involved in ion translocation in ryanodine receptor channels. *Q. Rev. Biophys.* **34**, 61–104 (2001).
42. Welch, W., Rheault, S., West, D.J. & Williams, A.J. A model of the putative pore region of the cardiac ryanodine receptor channel. *Biophys. J.* **87**, 2335–2351 (2004).
43. Xu, L., Wang, Y., Gillespie, D. & Meissner, G. Two rings of negative charges in the cytosolic vestibule of type-1 ryanodine receptor modulate ion fluxes. *Biophys. J.* **90**, 443–453 (2006).
44. Samsó, M., Feng, W., Pessah, I.N. & Allen, P.D. Coordinated movement of cytoplasmic and transmembrane domains of RyR1 upon gating. *PLoS Biol.* **7**, e85 (2009).
45. Doyle, D.A. *et al.* The structure of the potassium channel: molecular basis of K^+ conduction and selectivity. *Science* **280**, 69–77 (1998).
46. Long, S.B., Campbell, E.B. & Mackinnon, R. Crystal structure of a mammalian voltage-dependent Shaker family K^+ channel. *Science* **309**, 897–903 (2005).
47. Payandeh, J., Scheuer, T., Zheng, N. & Catterall, W.A. The crystal structure of a voltage-gated sodium channel. *Nature* **475**, 353–358 (2011).

48. Li, P. & Chen, S.R. Molecular basis of Ca^{2+} activation of the mouse cardiac Ca^{2+} release channel (ryanodine receptor). *J. Gen. Physiol.* **118**, 33–44 (2001).
49. Shi, N., Ye, S., Alam, A., Chen, L. & Jiang, Y. Atomic structure of a Na^{+}- and K^{+}-conducting channel. *Nature* **440**, 570–574 (2006).
50. Zhou, Q. *et al.* Carvedilol and its new analogs suppress arrhythmogenic store overload-induced Ca^{2+} release. *Nat. Med.* **17**, 1003–1009 (2011).
51. Liu, N. *et al.* Arrhythmogenesis in catecholaminergic polymorphic ventricular tachycardia: insights from a RyR2 R4496C knock-in mouse model. *Circ. Res.* **99**, 292–298 (2006).
52. Sedej, S. *et al.* Na^{+}-dependent SR Ca^{2+} overload induces arrhythmogenic events in mouse cardiomyocytes with a human CPVT mutation. *Cardiovasc. Res.* **87**, 50–59 (2010).
53. Mitchell, R.D., Palade, P. & Fleischer, S. Spontaneous calcium release from sarcoplasmic reticulum. Assessment of other ionic influences. *J. Biol. Chem.* **259**, 1073–1081 (1984).
54. Fabiato, A. Two kinds of calcium-induced release of calcium from the sarcoplasmic reticulum of skinned cardiac cells. *Adv. Exp. Med. Biol.* **311**, 245–262 (1992).
55. Watanabe, H. *et al.* Flecainide prevents catecholaminergic polymorphic ventricular tachycardia in mice and humans. *Nat. Med.* **15**, 380–383 (2009).
56. Hilliard, F.A. *et al.* Flecainide inhibits arrhythmogenic Ca^{2+} waves by open state block of ryanodine receptor Ca^{2+} release channels and reduction of Ca^{2+} spark mass. *J. Mol. Cell. Cardiol.* **48**, 293–301 (2010).
57. Sitsapesan, R. & Williams, A. The gating of the sheep skeletal sarcoplasmic reticulum Ca^{2+}-release channel is regulated by luminal Ca^{2+}. *J. Membr. Biol.* **146**, 133–144 (1995).
58. Zhou, J., Launikonis, B.S., Rios, E. & Brum, G. Regulation of Ca^{2+} sparks by Ca^{2+} and Mg^{2+} in mammalian and amphibian muscle. An RyR isoform-specific role in excitation-contraction coupling? *J. Gen. Physiol.* **124**, 409–428 (2004).
59. Dabertrand, F., Mironneau, J., Macrez, N. & Morel, J.L. Full length ryanodine receptor subtype 3 encodes spontaneous calcium oscillations in native duodenal smooth muscle cells. *Cell Calcium* **44**, 180–189 (2008).

ONLINE METHODS

Site-directed mutagenesis. All single and double point mutations were introduced into the channel pore region of mouse RyR2 by the PCR-mediated overlap extension method, as described previously[40,48,60]. The NruI (14,237)-NotI (vector) fragment containing a mutation in the pore region was removed from the PCR product and was subcloned into full-length mouse RyR2 cDNA. PCRs were carried out in 100 µl reaction buffer containing 20 mM Tris-HCl (pH 8.8), 10 mM KCl, 1 mM $(NH4)_2SO_4$, 2.0 mM $MgSO_4$, 0.1% Triton X-100, 0.1 mg ml^{-1} BSA, 50 ng of each DNA primer, 200 µM each of dATP, dCTP, dGTP and dTTP (Amersham), 1 unit of Pfu DNA polymerase (Stratagene) and 100 ng of template cDNA. The DNA was denatured for 4 min at 94 °C followed by 30 cycles of amplification. Each cycle had the following reaction conditions: 94 °C for 45 s, 46–55 °C for 1 min (determined by the melting temperature of the primers) and then 72 °C for 2 min. An additional step of 5 min at 72 °C was applied after the 30th cycle of reaction. All mutations and the sequences of the PCR-amplified regions were confirmed by DNA sequencing. Full-length mouse WT and mutant RyR2 cDNAs were subcloned into the mammalian expression vector pcDNA3. We also sequenced the entire coding regions of WT, E4872A and E4872Q RyR2 cDNAs using 30 DNA primers; the sequences of the WT, E4872A and E4872Q cDNAs were identical except for the introduced mutations (data not shown).

DNA transfection and preparation of cell lysates. HEK293 cells grown on 100-mm tissue culture dishes in supplemented DMEM were transfected with WT or mutant RyR2 cDNA using Ca^{2+} phosphate precipitation, and cell lysates were prepared from transfected HEK293 cells as described previously[40,48]. Briefly, HEK293 cells grown for 24 h after transfection were washed with PBS (137 mM NaCl, 8 mM Na_2HPO_4, 1.5 mM KH_2PO_4 and 2.7 mM KCl) plus 2.5 mM EDTA and harvested in the same solution by centrifugation for 8 min at 700*g* in an IEC Centra-CL2 centrifuge. The cells were then washed with PBS without EDTA and centrifuged again at 700*g* for 8 min. The PBS-washed cells were solubilized in a lysis buffer containing 25 mM Tris, 50 mM HEPES (pH 7.4), 137 mM NaCl, 1% 3-[(3-cholamidopropyl)dimethylammonio]-1-propanesulfonate (CHAPS), 0.5% soybean phosphatidylcholine, 2.5 mM dithiothreitol (DTT) and a protease inhibitor mix (1 mM benzamidine, 2 mg ml^{-1} leupeptin, 2 mg ml^{-1} pepstatin A, 2 mg ml^{-1} aprotinin and 0.5 mM PMSF). This mixture was incubated on ice for 1 h. Cell lysates were obtained by centrifuging twice at 16,000*g* in a microcentrifuge at 4 °C for 30 min to remove unsolubilized material.

[^{3}H]ryanodine binding. Cells were grown to 95% confluence in a 75-cm^2 flask, split with PBS and plated in 100-mm tissue culture dishes at ~10% confluence 18–20 h before transfection with WT and mutant cDNAs. After transfection for 24 h, the cells were harvested and lysed in lysis buffer containing 25 mM Tris, 50 mM HEPES, pH 7.4, 137 mM NaCl, 1% CHAPS, 0.5% egg phosphatidylcholine, 2.5 mM DTT and a protease inhibitor mix (1 mM benzamidine, 2 µg ml^{-1} leupeptin, 2 µg ml^{-1} pepstatin A, 2 µg ml^{-1} aprotinin and 0.5 mM PMSF) on ice for 60 min. Cell lysates were obtained after removing unsolubilized material by centrifugation twice in a microcentrifuge at 4 °C for 30 min each. Equilibrium [^{3}H]ryanodine binding to cell lysates was performed as described previously[48] with some modifications. [^{3}H]ryanodine binding was carried out in a total volume of 300 µl binding solution containing 30 µl of cell lysate, 100 mM KCl, 25 mM Tris, 50 mM HEPES (pH 7.4), 5 nM [^{3}H]ryanodine and a protease inhibitor mix at 37 °C for 20 min. Different ratios of $CaCl_2$ and ethylene glycol tetraacetic acid (EGTA) were added to set free [Ca^{2+}] in a range from pCa 9.89 to pCa 4. The ratio of Ca^{2+} to ethylene glycol tetraacetic acid (EGTA) was calculated using the computer program of Fabiato and Fabiato[61]. The binding mix was diluted with 5 ml of ice-cold washing buffer containing 25 mM Tris, pH 8.0, and 250 mM KCl and immediately filtered through Whatman GF/B filters presoaked with 1% polyethylenimine. The filters were washed three times and radioactivity associated with the filters was determined by liquid scintillation counting. Nonspecific binding was determined by measuring [^{3}H]ryanodine binding in the presence of 50 mM unlabeled ryanodine. All binding assays were done in duplicate.

Single-channel recordings in lipid bilayers. Recombinant WT and mutant RyR2 channels were purified from cell lysates prepared from HEK293 cells transfected with WT or mutant RyR2 cDNA by sucrose density gradient centrifugation, as described previously[48,62]. Heart phosphatidylethanolamine (50%) and brain phosphatidylserine (50%) (Avanti Polar Lipids), dissolved in chloroform, were combined, dried under nitrogen gas and resuspended in 30 µl of *n*-decane at a concentration of 12 mg lipid per ml. Bilayers were formed across a 250-µm hole in a Delrin partition separating two chambers. The *trans* chamber (800 µl) was connected to the head stage input of an Axopatch 200A amplifier (Axon Instruments). The *cis* chamber (1.2 ml) was held at virtual ground. A symmetrical solution containing 250 mM KCl and 25 mM HEPES (pH 7.4) was used for all recordings, unless indicated otherwise. A 4-µl aliquot (~1 µg of protein) of sucrose density gradient–purified recombinant WT or mutant RyR2 channels was added to the *cis* chamber. Spontaneous channel activity was always tested for sensitivity to EGTA and Ca^{2+}. The chamber to which the addition of EGTA inhibited the activity of the incorporated channel presumably corresponds to the cytosolic side of the Ca^{2+} release channel. The direction of single channel currents was measured from the luminal to the cytosolic side of the channel, unless mentioned otherwise. Recordings were filtered at 2,500 Hz. Data analyses were carried out using the pCLAMP 8.1 software package (Axon Instruments). Free Ca^{2+} concentrations were calculated using the computer program of Fabiato and Fabiato[61].

Caffeine-induced Ca^{2+} release measurements. The free cytosolic Ca^{2+} concentration in transfected HEK293 cells was measured using the fluorescence Ca^{2+} indicator dye Fluo-3 AM, as described previously[39,48]. HEK293 cells grown on 100-mm tissue culture dishes for 18–20 h after subculture were transfected with 12–16 µg of WT or mutant RyR2 cDNA. Cells grown for 18–20 h after transfection were washed four times with PBS and incubated in KRH buffer without $MgCl_2$ and $CaCl_2$ (KRH buffer: 125 mM NaCl, 5 mM KCl, 1.2 mM KH_2PO_4, 6 mM glucose, 1.2 mM $MgCl_2$, 2 mM $CaCl_2$ and 25 mM HEPES, pH 7.4) at room temperature for 40 min and at 37 °C for 40 min. After being detached from culture dishes by pipetting, cells were collected by centrifugation at 1,000 r.p.m. for 2 min in a Beckman TH-4 rotor. Cell pellets were washed twice with KRH buffer and loaded with 10 µM Fluo-3 AM in KRH buffer plus 0.1 mg ml^{-1} BSA and 250 µM sulfinpyrazone at room temperature for 60 min, followed by washing with KRH buffer three times and resuspension in 150 µl KRH buffer plus 0.1 mg ml^{-1} BSA and 250 µM sulfinpyrazone. The Fluo-3 AM–loaded cells were added to 2 ml (final volume) KRH buffer in a cuvette. The fluorescence intensity of Fluo-3 AM at 530 nm was measured before and after repeated additions or single additions of various concentrations of caffeine in an SLM-Aminco series 2 luminescence spectrometer with 480-nm excitation at 25 °C (SLM Instruments). The peak levels of each caffeine-induced Ca^{2+} release were determined and normalized to the highest level (100%) of caffeine-induced Ca^{2+} release for each experiment. The normalized data were fitted with the Hill equation to calculate the K_{caff} value for each experiment, defined as the caffeine concentration that produces 50% of the highest caffeine-induced Ca^{2+} release. The K_{caff} value of each mutant was then compared with that of WT RyR2 to generate the ratio of K_{caff}(mut) to K_{caff}(WT).

Generation of stable, inducible HEK293 cell lines. Stable, inducible HEK293 cell lines expressing WT and mutant RyR2 were generated using the Flp-In T-REx core kit from Invitrogen[14,26]. Briefly, full-length cDNA encoding the WT or mutant RyR2 channel was subcloned into the inducible expression vector pcDNA5/FRT/TO. Flp-In T-REx-293 cells were then co-transfected with the inducible expression vector pcDNA5/FRT/TO containing WT or mutant RyR2 cDNA and the pOG44 vector encoding the Flp recombinase in a 1:5 ratio using the Ca^{2+} phosphate precipitation method. Transfected cells were washed with PBS (137 mM NaCl, 8 mM Na_2HPO_4, 1.5 mM KH_2PO_4 and 2.7 mM KCl) 1 d after transfection and allowed to grow for an additional 1 d in fresh medium. The cells were then washed again with PBS, harvested and plated onto new dishes. After the cells had attached (~4 h), the growth medium was replaced with a selective medium containing 200 µg ml^{-1} hygromycin (Invitrogen). The selective medium was changed every 3–4 d until the desired number of cells was obtained. The hygromycin-resistant cells were pooled, aliquotted and stored at −80 °C.

Single-cell Ca^{2+} imaging of HEK293 cells. Intracellular cytosolic Ca^{2+} changes in stable, inducible HEK293 cells expressing WT or mutant RyR2

channels were monitored using single-cell Ca^{2+} imaging and the fluorescent Ca^{2+} indicator dye Fura-2 AM, as described previously[14,26]. Briefly, cells grown on glass coverslips for 18–22 h after induction by 1 μg ml^{-1} tetracycline were loaded with 5 μM Fura-2 AM in KRH (Krebs-Ringer-HEPES) buffer (125 mM NaCl, 5 mM KCl, 1.2 mM KH_2PO_4, 6 mM glucose, 1.2 mM $MgCl_2$ and 25 mM HEPES, pH 7.4) plus 0.02% Pluronic F-127 and 0.1 mg ml^{-1} BSA for 20 min at room temperature (23 °C). Coverslips were then mounted in a perfusion chamber (Warner Instruments) on an inverted microscope (Nikon TE2000-S). The cells were continuously perfused with KRH buffer containing increasing extracellular Ca^{2+} concentrations (0.2–2.0 mM). Increasing the extracellular Ca^{2+} concentration will lead to increased Ca^{2+} entry and subsequent Ca^{2+} loading of internal stores; when store Ca^{2+} content reaches a threshold level, the RyR2 opens, resulting in a spontaneous Ca^{2+} release event. Caffeine (10 mM) was applied at the end of each experiment to confirm the expression of active RyR2 channels. Time-lapse images (0.5 frames per s) were captured and analyzed with Compix Simple PCI 6 software (Compix Inc.). Fluorescence intensities were measured from regions of interest centered on individual cells. Only cells that responded to caffeine were used in analyses. All chemicals were obtained from Sigma unless otherwise specified.

Culture, transfection and single-cell Ca^{2+} imaging of HL-1 mouse cardiac cells. HL-1 cardiac cells were kindly provided by W.C. Claycomb from the Louisiana State University Health Sciences Center. Cells were thawed and grown in a 75-cm^2 tissue culture flask coated with 0.02% (wt/vol) gelatin in Claycomb medium (JRH Biosciences) supplemented with 10% (vol/vol) FBS, penicillin-streptomycin (100 U ml^{-1} and 100 μg ml^{-1}, respectively), 2 mM L-glutamine and 0.1 mM norepinephrine. For transfection, HL-1 cells (~3×10^6 cells) were washed with PBS and collected in a 13-ml Falcon tube. The cells were then centrifuged at 1,200 r.p.m. for 2 min and the supernatant was removed. The cell pellet was then gently mixed with 10 μg of WT or mutant RyR2 cDNA in Cell Line Nucleofection Solution V (Lonza) in a total volume of 100 μl. The mixture of cells and DNA was subjected to nucleofection using an Amaxa apparatus with the A033 program. Transfected cells were then plated onto a 12-well plate containing 12-mm glass coverslips coated with gelatin and fibronectin and grown for 24–28 h. Intracellular Ca^{2+} transients in transfected HL-1 cells were measured by single-cell Ca^{2+} imaging and the fluorescence Ca^{2+} indicator dye Fura-2 AM. Briefly, cells grown on glass coverslips for 24–28 h after transfection were loaded with 5 μM Fura-2 AM in a modified KRH buffer (125 mM NaCl, 5 mM KCl, 6 mM glucose, 1.2 mM $MgCl_2$ and 25 mM HEPES (pH 7.4) without KH_2PO_4), plus 0.02% Pluronic F-127 (Molecular Probes) and 0.1 mg ml^{-1} BSA for 20 min at room temperature. The coverslips were then mounted in a perfusion chamber (Warner Instruments) on an inverted microscope (Nikon TE2000-S). The cells were perfused continuously with KRH buffer containing different concentrations of $CaCl_2$ (0–10 mM) at room temperature (23 °C). Time-lapse images (0.5 frames per s) were captured through an S-Fluor ×20/0.75 objective and a Chroma filter set using the Simple PCI System. Data were analyzed with Compix Simple PCI 6 software (Compix).

Single-cell Ca^{2+} imaging of mouse ventricular myocytes. Mouse hearts were mounted on the Langendorff apparatus and single ventricular myocytes were isolated using the collagenase type II (Worthington Biochem) and protease method described previously[63]. Ventricular myocytes were placed on glass coverslips coated with laminin and loaded with 5 μM Fluo-4 AM (Invitrogen) plus 0.02% Pluronic F-127 in KRH buffer (125 mM NaCl, 5 mM KCl, 1.2 mM KH_2PO_4, 6 mM glucose, 1.2 mM $MgCl_2$ and 25 mM HEPES, pH 7.4) containing 1 mM Ca^{2+} for 20 min at room temperature (23 °C). Myocytes were washed for 10 min with KRH solution containing 1.0 mM Ca^{2+}. An additional 20 min was allowed for de-esterification of the Fluo-4 AM indicator. The Ca^{2+} concentration was then stepped to 3, 6, 10 and 15 mM to induce SOICR, which led to the formation of propagating global Ca^{2+} waves. Time-lapse images were captured at 10 frames per s and analyzed with Compix Simple PCI 6 software. Fluorescence intensities were measured from small rectangular regions of interest in each cell. All rod-shaped ventricular myocytes in the entire area imaged with a 10× or 20× objective were included in the analysis. For comparing resting cytosolic Ca^{2+} levels in WT and E4872Q heterozygous mutant ventricular myocytes, we used the fluorescent Ca^{2+} indictor Fura-2 AM. The cells were loaded with 5 μM Fura-2 AM (Molecular Probes) plus 0.02% Pluronic F-127 on a laminin-precoated coverslip for 20 min at room temperature. The coverslip was then placed in a perfusion chamber mounted onto an inverted microscope (Nikon TE2000-S) equipped with an S-Fluor 20×/0.75 objective. The cells were then continuously perfused with KRH buffer containing 1.8 mM Ca^{2+}. Time-lapse fluorescent images (1 frame per s) of Fura-2 AM–loaded WT and mutant cells before, during and after a 30-s field stimulation at 1 Hz were captured at 510-nm emission with excitations at 340 and 387 nm using a charge-coupled device (CCD) camera and Compix Simple PCI 6 software.

Laser scanning confocal imaging of single ventricular myocytes. Mouse ventricular myocytes isolated from WT or RyR2 mutant mice were loaded with Rhod-2 AM (5 μM) for 20 min at room temperature[64]. After 20 min of de-esterification, the cells were placed in a recording chamber and perfused with normal Tyrode solution (1.8 mM Ca^{2+}) at 35–37 °C. Confocal Ca^{2+} imaging was performed in line-scan mode with a laser scanning confocal microscope (LSM 510, Carl Zeiss) equipped with a numerical aperture (NA) 1.35, 63× lens. Images of depolarization-induced Ca^{2+} transients and caffeine-induced Ca^{2+} transients (SR Ca^{2+} contents) were acquired at a sampling rate of 1.93 ms per line along the longitudinal axis of the myocytes. Steady-state Ca^{2+} transients were achieved by a 30-s pacing at 1, 3 or 5 Hz. SR Ca^{2+} content was determined after steady-state stimulation at 1 Hz by measuring the amplitude of Ca^{2+} release induced by local delivery of 20 mM caffeine. All digital images were processed with IDL 6.0 (Research System Inc.).

Simultaneous recordings of depolarization-induced Ca^{2+} currents and Ca^{2+} transients under voltage clamp. Simultaneous recording of voltage-clamp Ca^{2+} currents and Ca^{2+} transients were performed at 35–37 °C in the ruptured whole-cell configuration. Voltage and current signals were measured with an Axon 200B patch-clamp amplifier controlled by a personal computer using a Digidata 1440A acquisition board driven by pCLAMP 10.0 software (Axon Instruments). The Ca^{2+} indicator Rhod-2 pentapotassium salt (100 μM) was dialyzed into the cells in a pipette solution containing (in mmol per liter) 110 CsCl, 20 tetraethylammonium chloride (TEACl), 10 NaCl, 0.4 Na-GTP, 5 Mg-ATP, 10 HEPES and 1 $MgCl_2$, pH adjusted to 7.2 with CsOH. The bath solution contained (in mmol per liter) 140 NaCl, 5 KCl, 0.5 $MgCl_2$, 1.8 $CaCl_2$, 0.33 NaH_2PO_2, 10 glucose and 10 HEPES, pH adjusted to 7.4 with NaOH. After establishment of the whole-cell mode, the cells were switched to the recording bath solution containing (in mmol per liter) 140 NaCl, 10 CsCl, 1 $MgCl_2$, 1.8 $CaCl_2$, 0.33 NaH_2PO_4, 10 glucose, 10 HEPES and 0.02 tetrodotoxin (TTX), pH 7.4. The cells were clamped to a holding potential of −80 mV, followed by a ramp depolarization to −40 mV from −80 mV (600 ms) and a holding command at −40 mV for 100 ms before application of voltage command steps ranging from −40 mV to 50 mV in 10-mV increments (300 ms). The voltage commands were applied at 15-s intervals. Confocal images of depolarization-induced Ca^{2+} transients were acquired at a sampling rate of 1.92 ms per line (512 pixels per line × 1,000 lines) with the scanline along the long axis of the ventricular myocytes.

Voltage-clamp recordings of I_{NCX} in WT and E4872Q heterozygous cardiac myocytes. Experiments were performed at 37 °C. Na-Ca exchange (NCX) currents (I_{NCX}) were recorded with an Axon-200B patch-clamp amplifier and a Digidata 1400A data acquisition system controlled by pCLAMP10.0 software (Axon Instruments). The pipette solution contained (in mM) 110 CsCl, 20 TEACl, 10 NaCl, 5 Mg-ATP, 10 HEPES, 0.4 $MgCl_2$, 2.5 $CaCl_2$ and 5 EGTA, pH adjusted to 7.2 with CsOH (final Ca^{2+} concentration, 108 nM). The bath solution contained (in mmol per liter) 140 NaCl, 5 KCl, 1 $MgCl_2$, 1.8 $CaCl_2$, 10 glucose, 10 HEPES, 10 CsCl, 0.01 ouabain, 0.01 verapamil and 0.1 niflumic acid, pH adjusted to 7.4 with NaOH. After establishment of the whole-cell mode, the cells were clamped at a holding potential of −80 mV. A descending voltage ramp polarization from +80 mV to −120 mV at 100 mV per s followed by instant return to the holding potential of −80 mV was used. The voltage command was repeated at 10-s intervals. I_{NCX} was measured as the current sensitive to 5 mM Ni^{2+}.

doi:10.1038/nm.3440

***In situ* confocal Ca^{2+} imaging of intact hearts.** Excised hearts were perfused with Rhod-2 AM (0.3 mM) containing Kreb-Henseleit's (KH) solution (in mM: 120 NaCl, 24 $NaHCO_3$, 11.1 glucose, 5.4 KCl, 1.8 $CaCl_2$, 1 $MgCl_2$, 0.42 NaH_2PO4, 10 taurine and 5 creatine, oxygenated with 95% O_2 and 5% CO_2) at room temperature for 30 min using a retrograde Langendorff perfusion system[65]. Hearts were later transferred to another Langendorff apparatus (37 °C) attached to the confocal microscope system after Rhod-2 AM loading was completed. The heart was placed onto a recording chamber for *in situ* confocal (line-scan) imaging of Ca^{2+} signals from epicardial myocytes under sinus rhythm. To avoid motion artifacts during Ca^{2+} imaging, blebbistatin (10 μM; Sigma) and BDM (2,3-butandion-monoxim; 10 mM; Sigma) were added to the perfusion solution. The confocal line-scan images were acquired at a rate of 1.93 ms per line. Ca^{2+} transients were autonomously elicited by electrical signals from the sinus atrial node. After perfusion in KH solution containing 1.8 mM Ca^{2+}, the heart was switched to a solution containing 3–10 mM Ca^{2+} to induce SOICR.

Animal studies. All animal studies were approved by the Institutional Animal Care and Use Committees at the University of Calgary, the University of Iowa, Rush University Medical Center and the University of California at San Diego and were performed in accordance with US National Institutes of Health guidelines. Adult RyR2 mutant mice and WT control littermates (8–12 weeks of age) of both sexes were used for all experiments.

Generation of a knock-in mouse strain harboring the RyR2 E4872Q mutation. A genomic DNA phage clone containing part of the mouse RyR2 gene was isolated from a lambda mouse 129-SV/J genomic DNA library (Stratagene) and used to construct the RyR2 E4872Q knock-in targeting vector. This genomic DNA fragment (~15 kb) was released from the lambda vector by NotI and was subcloned into pBluescript to form the plasmid RyR2-WT-BS. PCR-based site-directed mutagenesis was performed to generate a 980-bp DNA fragment containing the E4872Q mutation in exon 101 using the RyR2-WT-BS plasmid as a template. A HindIII site was created in the 5′ region and an XhoI site was created in the 3′ region of this DNA fragment, which was then subcloned using HindIII and XhoI into a targeting vector containing a neomycin (neo) selection cassette flanked by FRT sites. A 6,106-bp KpnI-ApaI genomic DNA fragment containing exon 101 was isolated from the RyR2-E4872Q-BS plasmid and inserted into the targeting vector with NotI and SalI sites. The DNA sequences of all exons and PCR fragments used for constructing the targeting vector were confirmed by DNA sequencing. The targeting vector was linearized with KpnI and subsequently electroporated into R1 embryonic stem (ES) cells at the Mouse Facility at the University of California, San Diego (UCSD).

G418-resistant ES clones (480 clones) were screened for homologous recombination by Southern blotting. Briefly, genomic DNA was extracted from G418-resistant ES cell clones using a DNeasy tissue kit (Qiagen). ES cell DNA was digested using Bsu36I, separated on a 1% (wt/vol) agarose gel and subsequently blotted onto a nitrocellulose membrane. The DNA probe, a 900-bp DNA fragment, was generated by PCR from mouse genomic DNA using the following primers: forward, 5′-CTGTTTCCGGAAACAGTCCCCTGC-3′ and reverse, 5′-AAGCATGGGATTCTATAATTTCCT-3′. The PCR product was subsequently radiolabeled using [^{32}P]dCTP by random priming (Invitrogen). DNA blots were hybridized with the radiolabeled probe and visualized by autoradiography. One positive homologous recombinant was detected and was microinjected into blastocysts from C57BL/6J mice to generate male chimeras at the Mouse Facility of UCSD. Male chimeric mice were bred with female Black Swiss mice to generate germline-transmitted heterozygous E4872Q-neo knock-in mice. RyR2-E4872Q-neo male mice were bred with female mice that express Flp recombinase to remove the selectable marker (neo). Genotypes from the F1 generation after removal of the neo cassette were determined by PCR using DNA from tail biopsy specimens using the DNeasy tissue kit from Qiagen and the following DNA primers: forward, 5′-GTTGGTAGATATTTCTCAGTCCACA-3′ and reverse, 5′-AACGTGGCAGGGCCGAATGATTACT-3′.

Echocardiography in conscious mice. To assess systolic and diastolic function, conscious 10- to 12-week-old E4872Q heterozygous mutant mice and their WT littermates were subjected to echocardiography as described previously by Semeniuk *et al.*[66]. The chest of the mouse was shaved and the mouse was restrained in a modified 50-ml tube with an opening for the echocardiographic probe. The mouse was allowed to rest for at least 15 min before echocardiography was performed using a Hewlett-Packard Sonus 4500 ultrasound machine (Agilent Technologies) with a frame rate of 300 frames per s. A 15-MHz linear transducer was placed on the left hemithorax interfaced with a layer of ultrasonic transmission gel (Aquasonic 100, Parker Laboratories), and the mice were imaged in a shallow left lateral decubitus position. The two-dimensional parasternal short-axis imaging plane was used as a guide for obtaining LV M-mode tracings close to the papillary muscle level. A minimum depth setting of 2 cm was used with a sweep speed of 100 mm s^{-1}. Doppler tracings of the mitral inflow and aortic outflow tract velocities were obtained in a modified parasternal long-axis view at a sweep speed of 100 mm s^{-1}, a sample volume length of 0.05 cm and a gate of 0.6 cm. Tracings were recorded on VHS videotape (Maxell) and printed on a Sony color printer (UP-5200, Sony). Data are the average of at least two separate scans, with each scan representing the average of three selected beats. All parameters were analyzed using the protocol described by Semeniuk *et al.*[66].

ECG recordings and induction of ventricular tachyarrhythmias in anesthetized mice. R4496C heterozygous mice, E4872Q R4496C compound heterozygous mice and their WT littermates were assessed for their susceptibility to drug-induced arrhythmias using ECG recordings. Briefly, mice (8–10 weeks old) were lightly anesthetized with isoflurane vapor (0.5–1%) and 95% O_2. Anesthetized mice were placed on a heating pad (27 °C), and subcutaneous needle electrodes were inserted into the right upper limb and left lower abdomen for ECG recordings (BIOPAC MP System). The animals' ECG recordings were monitored continuously under anesthesia until the heart rate became stabilized. A baseline ECG was recorded for 5–10 min. For induction of ventricular arrhythmias in E4872Q R4496C compound heterozygous mice and R4496C heterozygous mice, the mice were subjected to intraperitoneal injection of epinephrine (1.6 mg per kg body weight) and caffeine (120 mg per kg body weight). ECG was continuously recorded for 30 min after the infusion of epinephrine and caffeine.

Generation of RyR2 R4496C E4872Q compound heterozygous mice. To generate R4496C E4872Q compound heterozygous mice, we bred R4496C[50] heterozygous mice with E4872Q heterozygous mice. Although the exact distribution and stoichiometry of the R4496C and E4872Q mutant subunits in the tetrameric structure of RyR2 in R4496C E4872Q compound heterozygous mutant hearts is unknown, we assume that R4496C and E4872Q mutant subunits assemble randomly into a tetramer. If so, the likelihood of forming a tetramer with a specific composition of R4496C and E4872Q monomers would have the following distribution: R4496C homotetramers (1/16), three R4496C monomers plus one E4872Q monomer (4/16), two R4496C plus two E4872Q (6/16), one R4496C plus three E4872Q (4/16) and E4872Q homotetramers (1/16). Therefore, R4496C homotetramers would account for only 6.25% of all RyR2 tetramers in R4496C E4872Q compound heterozygous hearts. In other words, greater than 93% of RyR2 tetramers in R4496C E4872Q compound heterozygous hearts would be expected to contain one or more E4872Q subunits. Therefore, it is likely that the RyR2 E4872Q mutation exerts its protective effect on the hyperactive R4496C channel by forming heteromeric channels composed of E4872Q and R4496 subunits. As in the case of R4496C E4872Q compound heterozygous mice, we assume that the WT and E4872Q mutant monomers assemble randomly into tetramers, such that the likelihood of forming a tetramer with a specific composition of the WT and mutant monomers would have the following distribution: WT homotetramers with no E4872Q monomer (1/16), three WT monomers plus one E4872Q monomer (4/16), two WT plus two E4872Q (6/16), one WT plus three E4872Q (4/16) and E4872Q homotetramers (1/16). Therefore, WT homotetramers would be expected to account for only 6.25% of all RyR2 tetramers expressed in the E4872Q heterozygous cardiomyocytes. In other words, greater than 93% of RyR2 tetramers contain one or more E4872Q monomers in E4872Q heterozygous hearts. Thus, it is likely that the RyR2 E4872Q mutation exerts its negative effect on the function of RyR2 WT by forming heteromeric channels composed of E4872Q and WT subunits.

Immunoblotting analysis. Mouse hearts were crushed by a Wollenberger clamp precooled in liquid nitrogen. Crushed heart tissue was stored at −80 °C until use. Frozen cardiac tissue was pulverized in liquid nitrogen and homogenized immediately with a Brinkmann Polytron PT 15 homogenizer (setting 8, 4 bursts for 15 s each) in 6 volumes of 30 mM KH_2PO_4 (pH 7.0), 40 mM NaF, 5 mM EDTA, 300 mM sucrose, 4 μM leupeptin, 1 mM benzamidine, 100 μM PMSF and 0.5 mM DTT. Aliquots of homogenates were solubilized in 50 mM Tris-HCl (pH 7.4) plus 3% (wt/vol) SDS for 1 h at room temperature. Insoluble material was removed by centrifugation at 34,000*g* for 10 min. The protein concentration of the supernatant was determined using a Bio-Rad detergent-compatible protein assay kit. Solubilized proteins (20–30 μg) were used for SDS-PAGE[67]. SDS-PAGE resolved proteins were transferred to nitrocellulose membranes at 45 V for 18–20 h at 4 °C in the presence of 0.01% (wt/vol) SDS according to the method of Towbin *et al.*[68]. Nitrocellulose membranes containing the transferred proteins were blocked for 30 min with PBS containing 0.5% (vol/vol) Tween-20 and 5% (wt/vol) skim milk powder. The blocked membrane was incubated with antibodies against RyR2 (Thermo Scientific, Pierce ryanodine receptor monoclonal antibody, MA3-925, mouse, 1:1,000), SERCA2a (Santa Cruz Biotechnology, SERCA2 (C-20): sc-8094, goat, 1:10,000), CASQ2 (Thermo Scientific, calsequestrin antibody, PA1-913, rabbit, 1:2,500), triadin (Santa Cruz Biotechnology, triadin antibody (M-20): sc-33394, goat, 1:5,000), junctin (LifeSpan Biosciences Inc., junctin/ASPH rabbit anti-human polyclonal (N-terminus) (unconjugated) antibody, LS-C81640-LSBio, rabbit, 1:2,000) or β-actin (gift from J. Lytton, University of Calgary, rabbit, 1:5,000). The antibody-bound membrane was washed three times for 15 min with PBS containing 0.5% (vol/vol) Tween-20. The washed membrane was then incubated with secondary anti-mouse, anti-goat or anti-rabbit IgG (H&L) antibodies conjugated to horseradish peroxidase (1:20,000) for 30 min. After washing for 15 min three times, the bound antibodies were detected using an enhanced chemiluminescence kit from Pierce. The band intensities were analyzed using ImageJ software, and normalized to that of the β-actin band.

Modeling of the RyR2 ion-conducting pore. Welch *et al.*[42] determined the sequence of the ion-conducting pore of RyR2 and areas of sequence similarity between RyR2 and KcsA in the pore region, including the outer helix, pore helix, selectivity filter and inner helix. Using this as a guide, we used ClustalW[69] to align residues 4763–4881 of mouse RyR2 with residues from the KcsA (1BL8.pdb)[45], Kv1.2 (2A79.pdb)[46] and MthK (1LNQ.pdb)[70] potassium channels. The resulting alignment was refined manually. When compared to the potassium channel sequences, RyR2 contained a 10-residue insertion between the outer helix and pore helix and a 16-residue insertion between the selectivity filter and inner helix. We used SwissModel[71] to construct a homology model of the RyR2 ion permeation pore using the 1BL8 KcsA crystal structure as the modeling template. The two regions of insertions were modeled from loop databases[72]. The pore of RyR2 is known to have a cross-sectional diameter of approximately 7 Å (ref. 42), whereas that of KcsA is substantially smaller. To reproduce the experimentally-determined pore diameter, each subunit of the channel was shifted radially outwards from the long axis of the selectivity filter by 1.3 Å using a rigid body coordinate transformation. The tetrameric RyR2 pore model was energy minimized[72] to allow all bonds and bond angles to attain their optimized geometries. A series of point mutations were introduced into the model corresponding to the point mutations introduced experimentally. Each mutant RyR2 was subsequently energy minimized[72] to allow the mutated side-chain rotamers to adopt the lowest energy conformation. The electrostatic potential of the RyR2 model was calculated using the APBS[73] plugin for Visual Molecular Dynamics (VMD)[74]. Images were produced using VMD[74]. The backbone structure of the resultant RyR2 homology model is a close structural fit to the crystal structure of the NaK channel (PDB IDs 2AHY and 2AHZ)[49]. Although the overall channel fold of the NaK channel corresponds to that of KcsA, the N-terminal 19 residues of the NaK channel form an interfacial M0 helix, which is believed to lie at the lipid-water interface. Considering amino acids from the NaK M1 helix, P loop, P helix and M2 helix and disregarding loop regions, the root mean squared deviation between the NaK channel structure and the RyR2 pore model is 2.03 Å.

Statistical analyses. All values shown are the mean ± s.e.m. unless indicated otherwise. To test for differences between groups, we used Student's *t* test (two tailed). $P < 0.05$ was considered to be statistically significant.

60. Ho, S.N., Hunt, H.D., Horton, R.M., Pullen, J.K. & Pease, L.R. Site-directed mutagenesis by overlap extension using the polymerase chain reaction. *Gene* **77**, 51–59 (1989).
61. Fabiato, A. & Fabiato, F. Calculator programs for computing the composition of the solutions containing multiple metals and ligands used for experiments in skinned muscle cells. *J. Physiol. (Paris)* **75**, 463–505 (1979).
62. Jiang, D., Xiao, B., Zhang, L. & Chen, S.R. Enhanced basal activity of a cardiac Ca^{2+} release channel (ryanodine receptor) mutant associated with ventricular tachycardia and sudden death. *Circ. Res.* **91**, 218–225 (2002).
63. Hunt, D.J. *et al.* K201 (JTV519) suppresses spontaneous Ca^{2+} release and [^{3}H]ryanodine binding to RyR2 irrespective of FKBP12.6 association. *Biochem. J.* **404**, 431–438 (2007).
64. Guatimosim, S., Guatimosim, C. & Song, L.S. Imaging calcium sparks in cardiac myocytes. *Methods Mol. Biol.* **689**, 205–214 (2011).
65. Wei, S. *et al.* T-tubule remodeling during transition from hypertrophy to heart failure. *Circ. Res.* **107**, 520–531 (2010).
66. Semeniuk, L.M., Kryski, A.J. & Severson, D.L. Echocardiographic assessment of cardiac function in diabetic db/db and transgenic db/db-hGLUT4 mice. *Am. J. Physiol. Heart Circ. Physiol.* **283**, H976–H982 (2002).
67. Laemmli, U.K. Cleavage of structural proteins during the assembly of the head of bacteriophage T4. *Nature* **227**, 680–65 (1970).
68. Towbin, H., Staehelin, T. & Gordon, J. Electrophoretic transfer of proteins from polyacrylamide gels to nitrocellulose sheets: procedure and some applications. *Proc. Natl. Acad. Sci. USA* **76**, 4350–434 (1979).
69. Thompson, J.D., Higgins, D.G. & Gibson, T.J. CLUSTAL W: improving the sensitivity of progressive multiple sequence alignment through sequence weighting, position-specific gap penalties and weight matrix choice. *Nucleic Acids Res.* **22**, 4673–4680 (1994).
70. Jiang, Y. *et al.* Crystal structure and mechanism of a calcium-gated potassium channel. *Nature* **417**, 515–522 (2002).
71. Schwede, T., Kopp, J., Guex, N. & Peitsch, M.C. SWISS-MODEL: an automated protein homology-modeling server. *Nucleic Acids Res.* **31**, 3381–3385 (2003).
72. Guex, N. & Peitsch, M.C. SWISS-MODEL and the Swiss-PdbViewer: an environment for comparative protein modeling. *Electrophoresis* **18**, 2714–2723 (1997).
73. Baker, N.A., Sept, D., Joseph, S., Holst, M.J. & McCammon, J.A. Electrostatics of nanosystems: application to microtubules and the ribosome. *Proc. Natl. Acad. Sci. USA* **98**, 10037–10041 (2001).
74. Humphrey, W., Dalke, A. & Schulten, K. VMD: visual molecular dynamics. *J. Mol. Graph.* **14**, 33–38 (1996).

doi:10.1038/nm.3440